
Politecnico di Torino

**Politecnico di Torino**

---

Dipartimento di Ingegneria Ambientale e del territorio
Corso di Laurea magistrale in Ingegneria per l'Ambiente e il Territorio

# Remote sensing technologies for biomass estimation

Studente:
*Christian Barresi*

Corso:
*Remote sening*

---

Anno Accademico 2023-2024

# Contents

## List of Figures

# List of Tables

# 1 Abstract

Biomass estimation techniques can be broadly classified into two categories: ground-based and remote sensing methods. Ground-based methods, such as visual estimation and field spectrometry, are often time-consuming, costly, destructive, labor-intensive, and impractical for large-scale monitoring. Consequently, researchers have turned their attention to remote sensing methods that offer the advantages of spatio-temporal, large-scale, and rapid monitoring, and they are comparatively more cost-effective.

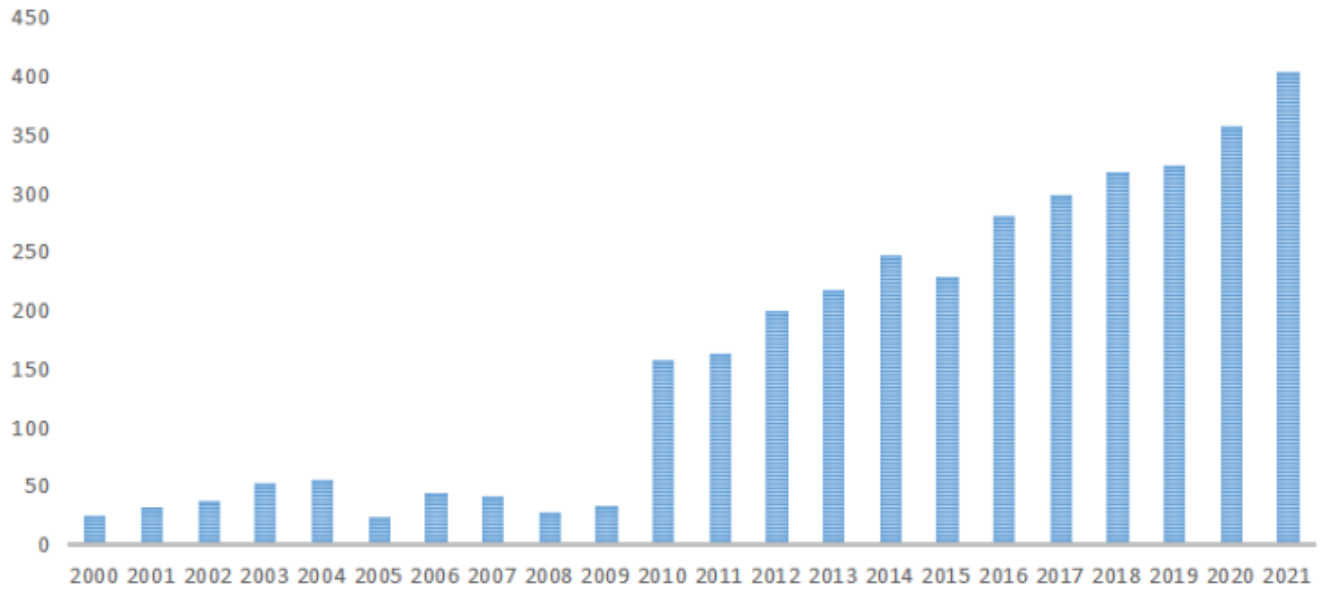


**Figure 1:** *Trends of Papers Published on space-borne CO2 Remote Sensing up to December 2021*

As a new monitoring method, remote sensing has been successfully applied in many sites with its advantages of extensive scope of observations, non-contact and long-term cost-effective monitoring. In this study, various remote sensing monitoring technologies are summarized and discussed in terms of their advantages and disadvantages in applications, their development trend in the future. The goal of the research is to obtain a model able to estimate the above ground biomass (AGB) over the forests of Alto-Adige region. The model utilises optical high resolution remote sensing data, acquired through PlanetScope missions, calibrated with the forest inventory informations at the municipality scale. Other than biomass, combining the advantages of satellite imagery with field data will provide a wealth of information that could be useful also for quantifying the various characteristics of trees, including canopy, structure and carbon storage. Researchers have assessed the capabilities of remotely sensed images obtained from various platforms, including unmanned aerial vehicles (UAVs), spaceborne satellites, and airborne sensors. Main categories, depending on the type of sensor used are summarized in the next sections.

# 2 Introduction

## 2.1 Optical images

High- and medium-resolution optical remote sensing are used for forest biomass estimation commonly. Generally, high-resolution optical images are too expensive, and the images are quite hard to obtain even though they have more accurate results of biomass estimation than medium-resolution optical images. Therefore, the medium-resolution satellite images (e.g., Landsat and Sentinel-2) are a better choice for forest biomass evaluation by different spatial scales due to their free accessibility and high suitability to landscape scale analysis. However, reducing the uncertainties is still a significant difficulty for biomass estimation using optical remote sensing data, especially when the study area has a high canopy. The information extracted from optical remote sensing is the radiation information of the canopy surface, which is easily affected by the complexity of forest crown layers [3]. Therefore, the precision problem is the biggest challenge of optical remote sensing in current remote sensing biomass estimation. Using high-resolution and hyperspectral remote sensing images will enhance biomass estimation accuracy, but the high price limits such data being widely utilized. Researchers prefer to choose free, open-source data, such as Landsat or Sentinel-2.

Landsat sensors, including Landsat-5, Landsat-7, and Landsat-8, have been utilized as multispectral satellite images for estimating biomass. Landsat-8 offers nine spectral bands with a spatial resolution of 30 m for Bands 1 to 7 and 9. The panchromatic band, Band 8, has a spatial resolution of 15 m. Different are the limitations associated with using Landsat satellite products as valuable sources for biomass estimation. Firstly, the 30 m spatial resolution of Landsat sensors makes it challenging to numerically evaluate the results and assess model validity against field measurements. Secondly, Landsat satellites have a 16-day revisit period, resulting in a relatively low temporal resolution, and thus, acquiring cloud-free, high-quality images becomes problematic [4].

The European Space Agency launched a high-resolution and multi-spectral imaging satellite, Sentinel-2A, in 2015 and Sentinel-2B in 2017. Sentinel-2 has thirteen spectral bands where four bands are configured at 10 m spatial resolution, six bands at 20 m, and three bands at 60 m spatial resolution, including four additional spectral bands strategically positioned in the red-edge region, which is a more sensitive band to vegetation. Sentinel-2 can revisit an area in 5 days by two satellites and it has a wide swath at 290 km. Compared to Landsat, Sentinel-2 has a double-satellite orbit and has four more bands. It is the unique one with three bands of data in the red edge range, which can efficiently obtain more rich geographical information. Studies have shown that Sentinel-2 is more suitable than Landsat for improving estimation accuracy [23]. The vegetation index extracted from near-infrared and red edge can strengthen the estimation accuracy. Many researches over the topic found that band 2 (blue), band 3 (green), band 5 (vegetation red edge), band 8 (NIR), and band 12 (SWIR) of Sentinel-2 had a strong correlation with biomass [3,4,13,23]. Data acquired from Multispectral Instrument (MSI) sensor onboard the Sentinel-2 satellites had been successfully used for quantifying the forage biomass in pastoral systems, providing

relatively accurate quantitative indicators of biomass in natural grassland areas of Shenandoah Valley, Virginia [4]. Unlike other multispectral satellite images, Sentinel-2 images excel in forage biomass estimation for two reasons. Firstly, its spatial resolution is suitable for studying paddocks of any size, including small dairy paddocks. Secondly, the five-day temporal resolution of Sentinel-2 enables continuous monitoring of rotational bale grazing and its impact on pasture growth, a crucial consideration for both dairy and beef industries [4]. Similar studies were also carried out in Monti Sibillini National Park, a 700 km2 protected area in central Italy, showing similar results [10].

However, optical imagery still has limitations in terms of estimating biomass. It relies on cloud-free weather conditions and it primarily captures reflectivity information from the top of the canopy, which may not fully represent a forest's structure, a critical factor related to biomass volume. Additionally, a saturation of surface reflectance and vegetation indices can occur in low to moderate spatial resolution products like Landsat, necessitating the utilization of alternative imagery platforms [4].

## 2.2 Active sensor radar data

Radar remote sensing is adopted to measure geometrical and dielectric attributes of forests. Radar has an intense penetration in vegetation, but the data processing is quite complicated, and the forest biomass has a different sensitivity to its wavelength. The most accurate radar systems operate with short wavelengths (i.e., X- and C-bands) [3]. However, the radar signal does not reach the ground because it is mainly backscattered by the canopy of the upper layer. Using long radar wavelengths (mainly L- and P-bands), the radar signal can penetrate the different layers from the top of the canopy to the ground. However, P-band radar imagery is expected to be available with the ESA BIOMASS mission to be launched in 2024.

Synthetic aperture radar (SAR), captured by Sentinel-1 satellites, provide insights into the backscattering properties of the vegetation structure, which can be correlated with biomass content. SAR data have a longer wavelength and stronger penetrating power compared with traditional optical remote sensing. Therefore, SAR data are more suitable for the estimation of the above-ground biomass (AGB) of forests. By incorporating SAR variables with the spectral indices, the models can leverage both optical and SAR data to estimate biomass. Unfortunately, since SAR is a side-view system, it causes nonlinear distortion in acquisition of areas with large terrain undulations, which could be resolved through geocoding operations [9].

## 2.3 Light detection and ranging (LiDAR) data

Light detection and ranging (LiDAR) is an active remote sensing technology that obtains the distance between a sensor and a target by calculating the time difference between the laser pulse emitted by the sensor and the received echo pulse. Because LiDAR has strong penetration into the forest, it can accurately obtain the three-dimensional structure information of forest tree height and canopy, thus realizing the leap from two-dimensional to three-dimensional forest canopy structure information, resulting

in the emergence of canopy parameters extracted from LiDAR data as a hot research topic globally [2]. The main LiDAR technology used in forest biomass estimation is backpack LiDAR and airborne LiDAR. Backpack LiDAR is hard to use for large-area assessment because the terrain and forestland accessibility easily influence it. Although airborne LiDAR is not limited by the terrain and can capture three-dimensional structure information; thus, it has a better performance for forest biomass estimation by improving the saturation problem in biomass estimation using optical remote sensing data. However, it still needs to be more suitable for large-area forest biomass estimation due to the limitation of the battery capacity and the increased imaging cost [3]. Moreover, LiDAR has no infrared signals, a limiting factor for vegetation analysis. Many studies addressed LiDAR technology and its potential, an example is the estimation of urban forest characteristic parameters using UAV-LiDAR coupled with canopy volume carried out in the Shenzhen area of southern China [2]. The results of the study provide an important reference for the estimation of single tree characteristic parameters in urban forests based on UAV-Lidar data.

LiDAR data acquisition includes terrestrial laser scanning (TLS), airborne laser scanner (ALS) and UAV laser scanning (ULS). The laser radar scanner installed on the TLS ground support obtains a high-density point cloud, but it takes a great deal of time to collect TLS data [7]. due to its static properties, so its use cannot be widely promoted. ALS can obtain a wide range of 3D point cloud data, but low point cloud density makes it impossible to accurately express object structure. Conversely, ULS can efficiently acquire large-area point cloud data, and compared with ALS, ULS flies at lower altitudes and can acquire a higher point cloud density. However, there are few studies on the extraction of single tree 3D green volume based on ULS.

The study that aimed to estimate 3D green volume and aboveground biomass of urban forest trees by UAV-LiDAR in Zhejiang province of China [7], showed a strong accuracy of the AGB estimated by ALS compared to ULS, the lower flight altitude of the ULS (60 m) compared with that of the ALS, enabled a higher density of point cloud data to be acquired, and higher density point cloud data helped to reconstruct the forest 3D structure at a more refined scale. Previous studies have shown that LiDAR pulses are nearly vertical, resulting in the number of point clouds from the lower parts of the crown being lower than those nearer the top, and, thus, ALS tends to underestimate the 3D green volume at the bottom of the canopy. Although the point cloud density obtained by ULS is higher than that of ALS, there is still a problem of missing point clouds inside the bottom layer of the canopy [7].

Another study focused on the Trentino Alto-Adige and Veneto regions [11], in northern Italy comparing data based on an airborne LiDAR survey conducted in 2014 by the Autonomous Province of Trento with an OPTECH ALTM 3100 sensor, which returned a point cloud with a minimal point density of 8 points/m2, with different combinations of ALOS2 (Advanced Land Observing Satellite-2), Copernicus Sentinel 1 and Sentinel 2 remote sensing data to estimate biomass loss caused by the Vaia windthrow. The results of this study show that in an alpine area, LiDAR (when available) is the best choice to quantify biomass loss and was considered the reference dataset; it suffers from less limitations and has

usually high accuracy, but for biomass quantification purpose it is useful only if coupled with proper ground data, allowing to build an estimate [11]. Pro and cons of each technology are then recaped in the next sections:

## 2.4 Advantages

Landsat (optical):

- free, open-source data;
- high suitability to landscape scale analysis;

Sentinel (optical):

- free, open-source data;
- better spatial and temporal resolution (5 days);
- suitable for biomass estimation;
- additional sensors in red-edge region;

Active sensor radar data:

- intense penetration in vegetation;
- wavelength adjustment for different penetration intensity;
- recorded backscattering properties suitable for biomass estimation;
- radar data could incorporate optical data for better estimation of biomass

LiDAR:

- strong penetration into the vegetation;
- three-dimensional structure information of forest tree height and canopy;
- sensor implemented by different supports;
- improves the saturation problem in biomass estimation using optical data;

## 2.5 Disadvantages

Landsat (optical):

- uncertainties for biomass estimation;
- low spatial resolution (30m);
- low temporal resolution (16 days);

- relies on cloud-free weather condition;

Sentinel (optical):

- relies on cloud-free weather condition;
- reflectivity information only from the top of the canopy;

Active sensor radar data:

- processing of data complicated;
- distortion in acquisition of areas with large undulations;

LiDAR:

- limited battery capacity for large area analysis;
- high cost for acquisition;
- no infrared signals;
- non homogeneous point cloud density acquisition from bottom and top part of canopy;

## 2.6 Spectral indices

A spectral index is a mathematical combination of two or more wavelengths that enhances the information content of the data [20]. Spectral indices can be used to extract information about specific features or properties of the Earth's surface, such as vegetation density, soil moisture, or water quality. The majority of the studies about the estimation of above ground biomass, utilise these indices obtained from the spectral information of the remotely sensed image and through geographical weighted regression analysis their relationship with environmental parameters is defined.

To implement forest biomass estimation, vegetation indices (VI) have been employed in lots of research. The VI has been shown to be related to photosynthesis to some extent and directly proportional to biomass or yield [3]. The Normalized Difference Vegetation Index (NDVI), is obtained as the difference between the near-infrared (NIR) and red spectral bands:

$$NDVI = \frac{NIR - Red}{NIR + Red} \tag{1}$$

where *NIR* and *red* are the spectral reflectances measured in the near infrared and red wavebands respectively.

| Ecosystem | Typical NDVI value | Location |
|---|---|---|
| Boreal forest | 0.6-0.8 | Alaska |

| | | |
|---|---|---|
| Temperate forest | 0.3-0.7 | France |
| Costal forest | 0.88-0.92 | Solomon Island |
| Alpine pasture | 0-0.13 | Italy |
| Annual grassland | 0.15-0.30 | California |
| Desert | 0.06-0.12 | Sinai, Egypt |

**Table 1:** *Typical NDVI values for different ecosystems*

NDVI ranges from 0-1, values around 0 indicate bare soil with no vegetation cover or clouds insted values close to 1 indicate complete vegetation cover and high vigor. It is sensitive to vegetation's chlorophyll content and photosynthetic activity. NDVI strongly correlates with vegetation greenness and biomass, making it a valuable indicator for estimating pasture biomass. The Modified Normalized Difference Vegetation Index (MNDVI) is a modification of NDVI, in which the green band is incorporated instead of the red band [26]. The saturation effect in dense and highly productive vegetation is reduced, improving the index's sensitivity to changes in biomass. The Green Normalized Difference Vegetation Index (GNDVI) is similar to NDVI, but it uses the green band instead of the red band.

$$GNDVI = \frac{NIR - Green}{NIR + Green} \tag{2}$$

It is particularly useful in areas with vegetation stress or senescence, as it is less affected by factors such as soil background and leaf pigments other than chlorophyll. Regarding the Enhanced Vegetation Index (EVI), the red, near-infrared, and blue bands are combined, providing enhanced vegetation vigor and biomass sensitivity by considering variations in the canopy structure and leaf area

$$EVI = \frac{NIR - Red}{NIR + C_1 \cdot Red - C_2 \cdot Blue + L} \tag{3}$$

$L$ is the soil adjustment factor, in order to correct for soil noise effects (soil color, soil moisture, soil variability across regions, etc.), which tend to impact the results., $C_1$ and $C_2$ are coefficients that correct for aerosol scattering in the atmosphere. The standard EVI used by NASA in MODIS sensor: L=1, $C_1$=6 and $C_2$=7.5. Near-infrared Reflectance of Vegetation (NIRv), integrate the advantages of NDVI and near-infrared reflectance and in recent years was found to have a strong and stable correlation with Gross Primary Productivity (GPP), which quantifies the total amount of carbon assimilated by plants through photosynthesis per unit time. Moreover previous studies have shown that the EVI index also correlates with surface observation data in global GPP estimation [20]. The Green Chlorophyll Index (GCI) is a spectral index that focuses on the green band, and it provides an estimate of the chlorophyll content in vegetation.

$$GCI = \frac{NIR}{Green} - 1 \tag{4}$$

It is useful for assessing the health and physiological condition of vegetation, which is directly related to biomass production.

Other vegetation indices included the Excess Green Vegetation Index (ExG), the Excess Red Vegetation Index (ExR), and the difference between these indices (ΔExGR) [21]. Previous studies [22] showed that among all the variables, only the ΔExGR index had a significant relationship with carbon sequestration in the urban area of Isfahan metropolitan, located in the center of Iran.

The application of spectral indices, is a valuable source for biomass estimation but their use can lead to saturation problems, a phenomenon called saturation tendency, has been reported in many previous studies and confirms that the spectral variables, whether spectral indices or reflectance values, insufficiently contribute to biomass estimation in grassland areas [4]. Therefore, integrating the dataset could be a valuable source of information for biomass estimation. The study by Wang et al. is the only study that has specifically used the integration of Sentinel-1 and Sentinel-2 for biomass and Leaf Area Index (LAI) estimation in grassland areas [23]. They showed that integrating Sentinel-1 and Sentinel-2 has high potential in biomass estimation and LAI prediction in grassland areas. LAI index is commonly used to estimate foliage cover and to forecast crop growth and yield. It is obtained through the following empirical formula from Boegh et al (2002):

$$LAI = 3.618 \cdot EVI - 0.118 \tag{5}$$

Where EVI is the Enhanced Vegetation Index value. Another frequently used index is the Structure–Insensitive Pigment Index (SIPI), which characterizes the photosynthetic activity and pigment concentration in vegetation. Although they will bring a saturation problem, the vegetation indices extracted from near-infrared and red edge can strengthen the estimation accuracy. As shown in the study carried out in Shangri-La City, China, the band 2 (blue), band 3 (green), band 5 (vegetation red edge), band 8 (NIR), and band 12 (SWIR) of Sentinel-2 had a strong correlation with biomass [3]. However, there are some limitations in the use of methods that focus on spectral indices; for example the adaptability of the methods for different kind of scenarios and vegetation, since the correlation between physical processes and indices is affected by different ecosystem structures and climate conditions.

# 3 Materials and methods

## 3.1 Study area

This research focuses on the Alto-Adige region, which is one of the richest in Italy for its forest biomass content. According to the INFC institute (Inventario Nazionale delle Foreste e dei serbatoi forestali di Carbonio) on the region the total wooden area equals 375351 ha, with a forest cover of 45.80%. The most common forest categories are grouped in the following plot:


**Figure 2:** *Forest categories*

For the study to be representative of the whole region, study surfaces are selected around different ecosystems, in the valley and on the mountain slope and also in areas with different local climate, having various species abundance. In the next figure the main forest categories are mapped:

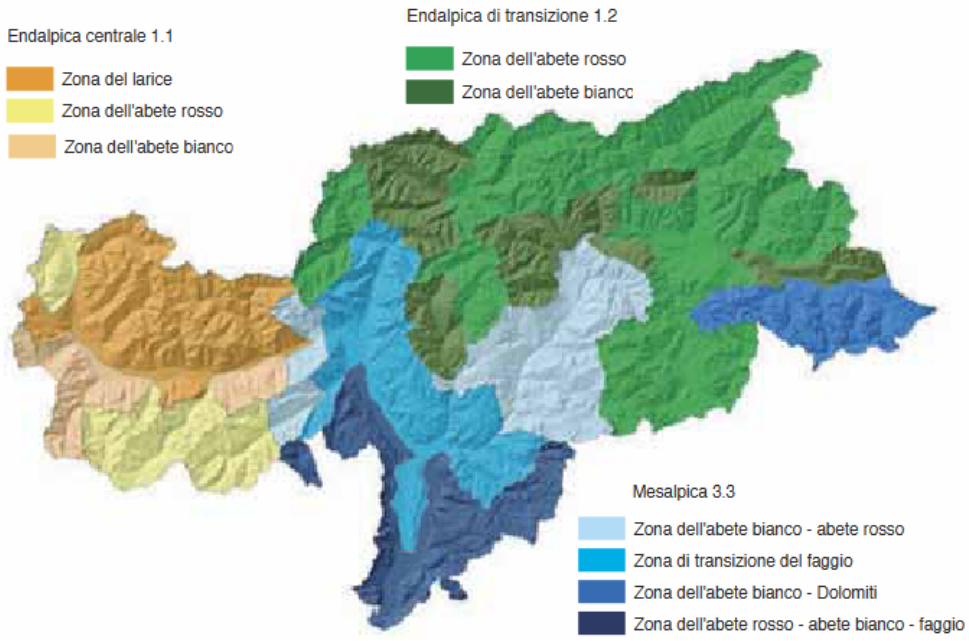


**Figure 3:** *Map of forest categories*

### 3.2 Transition endalpic district

Inside the transition endalpic district, the area of the white fir represents the transition between the endalpic region of the Norway spruce and the mesalpic region. The white fir shows a low competitiveness against the Norway spruce and is located mostly on the shady mountain's side. It is most common on the steep and shaded slopes and in the narrow valleys, is almost missing on the sunny slopes. The presence of the white fir is widely spread in the upper part of the Isarco valley, around the municipality of Bressanone, where it constitutes the dominant type. Because of the mining activity in the Ridanna and Racines valleys the species is almost absent in these areas. On the southern part of the Isarco valley the white fir area ends past Bressanone, where chestnuts and oaks are more diffused.

The presence of mountain and sub-alpine spruce forests is very typical of the Norway spruce area, locally it is very frequent to find larch trees, especially in the valleys around the main Alpine range. At low altitudes oak forests are concentrated. In general these environments are drier then the area of the white fir and the mesalpic district.

### 3.3 Mesalpic district

In this region the most common species at altitude between 200-500 m.a.s.l. for shaded slopes and until 700 m.s.s.l. for sunny sides are temperate oaks and hornbeams. In the sub-mountain area oaks and beech forests are common at altitude between 500-800 m.a.s.l., as long as mixed forest of chestnut and oaks especially on the shaded sides. Spruce forests can be found on shaded slopes at higher altitudes (800-1250 m.a.s.l.), instead on the sunny slopes beech and Scots pine are present, together with spruce trees in the more humid areas and spreading also at higher altitudes. Southern of the city of Bolzano, rainfall is more abundant, consequently the presence of beech and white spruce is dominant. In the valley part of the district chestunt trees are widely spread, also another characteristic of the mesalpic district is the presence of Norway spruce, Scots pine and larch fores in the areas where beech trees are absent. It is important to notice that the valley side of the area is witnessing a slow disappearance of Scots pine, gradually substituted by temperate oaks, whose habitat better fits this climate condition. This process is observed in other parts of the region as altitudinal planes are shifting toward higher altitude, as a result of climate change. Moreover a peculiar characteristic of this area is presence of broadleaf forests, which popolate the low altitudes, among the most common species hophornbeam, temperate oak and locust.

The available ground data used for the study was provided by the office of forest planning of the Alto-Adige region. The data is defined at the parcel scale, consequently 24 parcels were selected in different municipalities, in order to comprehend areas with various type of vegetation. The parcels locations fall inside 9 municipalities: Appiano, Cornedo, Fiè, Foresta, Nova Ponente, Racines, Renon, Velturno and Laives.

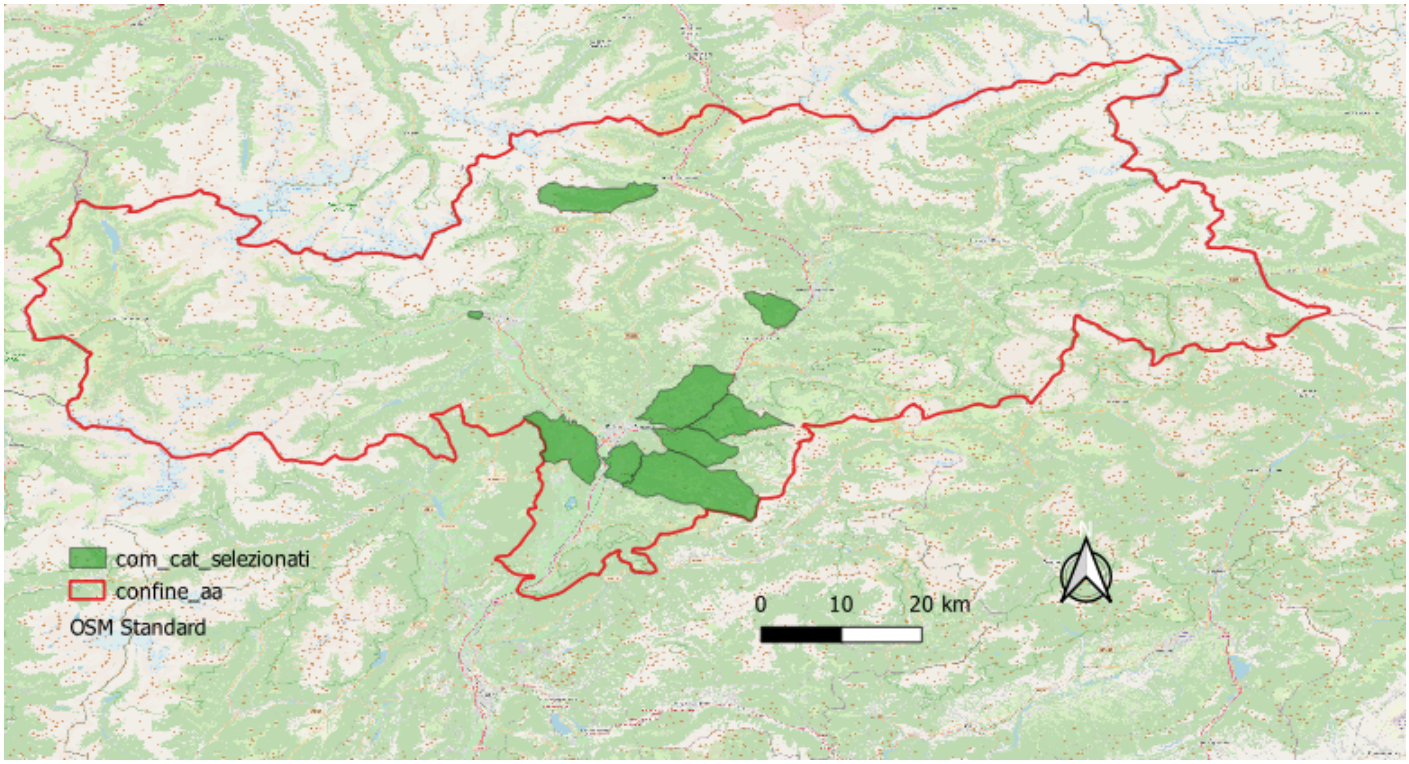


**Figure 4:** *Municipalities of the selected parcels*

The current law about forest management in Alto-Adige rules that all the properties with surface greater than 100 ha are managed by *plans*, these plans (more than 350 for the region) are issued by law and are valid for 10 years, in which they are continuously updated. They contain a detailed description of the property and its biometric characteristics together with all the planned activities for its maintenance. Instead, the selected properties have a surface smaller than 100 ha, therefore their management is obtained through *forest sheets*, in which all the measured properties of the forest are reported, they contain the indication of how much timber can be collected and the overall stock volume of the parcel. The forest stock volume (FSV, m3/ha) represents a fundamental variable for forest resources management and assessments on local, region and country scales and is the sum of the stem volumes of all the living trees per unit area. FSVs have a strong relationship with the aboveground biomass (AGB) and carbon stocks. In the provided data, the FSV is estimated by sampling several plots, which involves substantial manpower, materials, and financial resources.

## 3.4 Data survey

The field data used in this study derive directly from the region's database. Every 10 years the data for each particle are updated through a field survey, organized through sample areas, assumed to be representative of the whole land. The most basic information are obtained through visual inspection of an operator, instead biometric variables are determined through the implementation of the principle of dendrometry, the branch of forestry that is concerned with the measurement of the various dimensions of trees, such as their diameter, size, shape, age and more. The surveys are made both with callipering, the measurement of stem diameters with a calliper, but also through digital tools and specific softwares.

For the dendrometric surveys the procuedure used is the PNA (Prove di numerazione angolare), this method allows to quantify the number of trees per hectar in relation to their stem diameter [29]. Through the application of PNA to the sample area, matemathical and statistical relationships allow to obtain the mean stem diameter and the volume per hectar of the area.

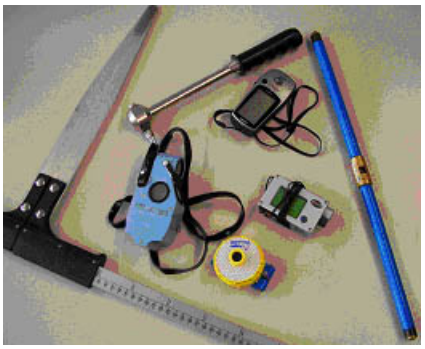

**Figure 5:** *Tools used by forest authorities in the surveys*

## 3.5 Dataset

The parcels selected are divided into coppice and high forest, most of them are labelled as high forest with few coppice parcels, today this form of government "intensive" has been replaced almost everywhere by the high forest, where the plants are left to grow old forests form capable of performing its functions slope protection.

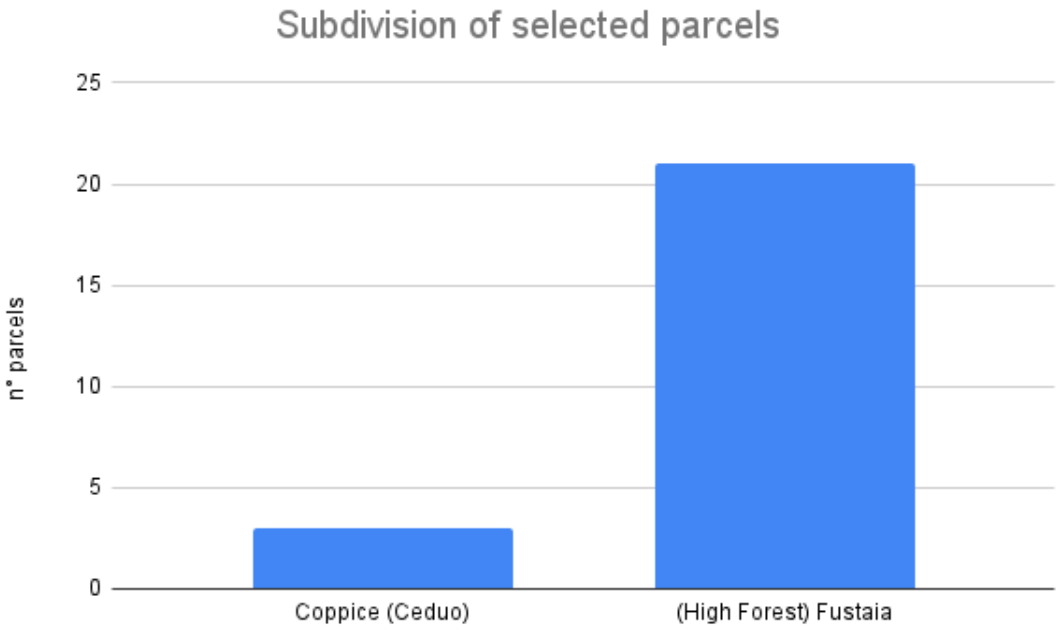


**Figure 6:** *Subdivision of parcels in coppice and high forest*

The surface value for each of the 24 polygons is represented in the next plot:

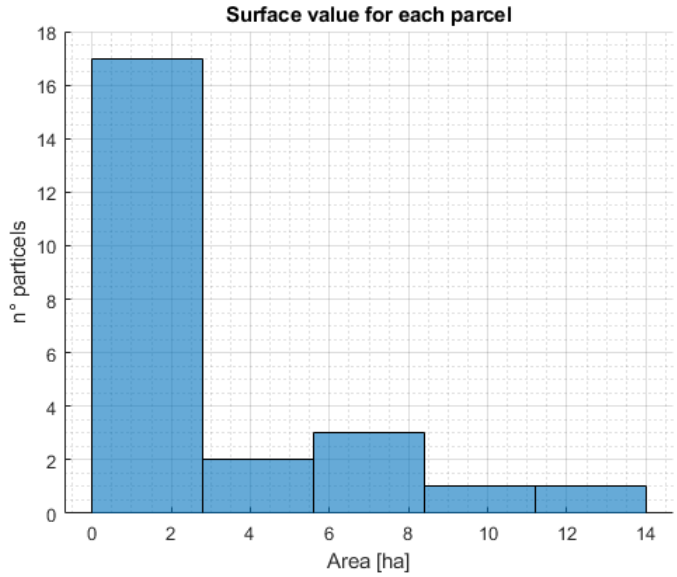


**Figure 7:** *Surface value for each parcel*

Additionally the basic information of the parcels selected are summarized in the table:

| | |
|---|---|
| N° parcels | 24 |
| Median (ha) | 1.48 |
| Maximum size (ha) | 13.58 |
| Minimum size(ha) | 0.02 |
| First quartile (ha,25%) | 0.56 |
| Third quartile (ha,75%) | 4.05 |
| Total area (ha) | 73.07 |

**Table 2:** *Basic information of polygons*

The most common three species found in the study areas are Abies alba, Picea abies, Larix decidua, Pinus sylvestris, Pinus nigra, Fagus sylvatica and in small part other broadleved. A certain type is considered dominant if its coverage is above 50% mark, sub dominant if its coverage ranges from 26%-50%, mixed for percentage between 5% and 25% and sporadic for coverage less than 5%. For any of the species, the characteristic parameters that allow the calculation of biomass are collected. For each parcel the stock volume is provided in the related forest sheet and is expressed both as total volume [m3] and specific volume [m3/ha]:

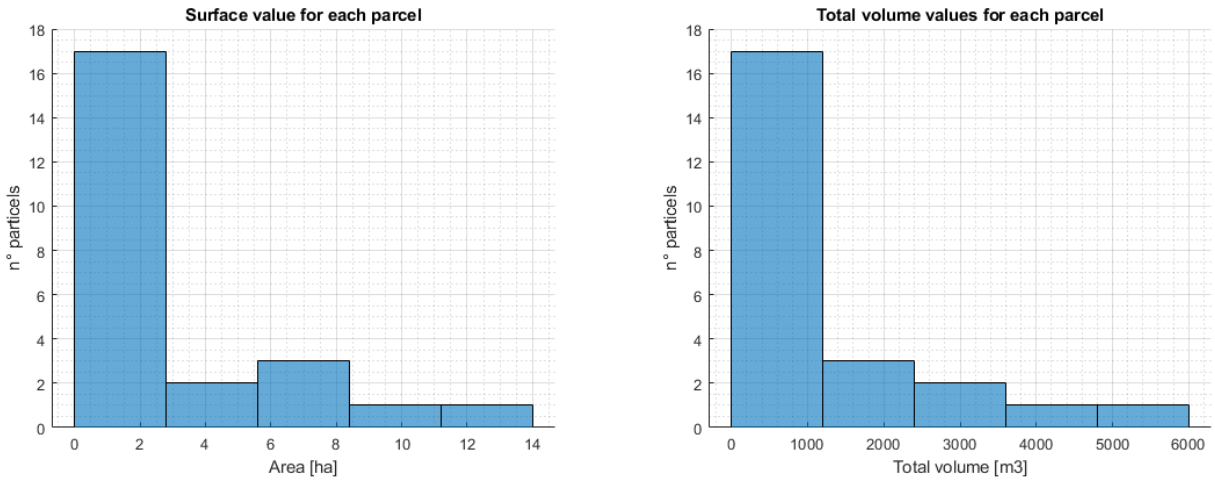


**(a)** *Specific volume* **(b)** *Total volume*

**Figure 8:** *Volume histograms for each particle*

Biomass can be calculated from the stock volume (V) data contained in the forest sheet by first estimating the wood density (WD) of the volume, which is a very important parameter to address the physical properties of the wood, it is a useful index of the effective quantity of wood in a specific sample. The wood density is also related to other fundamental properties of the wood, such as resistance and porosity, different are the methodologies for its estimation but the one that best fits the calculation of the biomass is the *basal density*[17], representing the ratio between dry weight of a sample and its volume at fresh state.

The wood density value needs to be expanded with a biomass expansion factor (BEF) to consider the biomass of the other aboveground components. Forest inventory data typically focus only on commercially important stem volume and rarely include quantitative estimates of other important biomass components such as root fractions, branches, leaves, which makes it necessary to estimate these elements of total biomass using expansion factors [27, 28]. However specific factors are not available at regional level so their value was assumed from literature [19]:

| Species | WD [Mg/m3] | BEF |
|---|---|---|
| Abies alba | 0.470 | 1.214 |
| Picea abies | 0.440 | 1.214 |
| Larix decidua | 0.507 | 1.18 |
| Pinus sylvestris | 0.453 | 1.196 |
| Pinus nigra | 0.507 | 1.196 |
| Fagus sylvatica | 0.527 | 1.195 |
| Other broadleved | 0.540 | 1.195 |

**Table 3:** *WD and BEF values for the most common tree species*

The following formula was eventually applied, using for each tree species the WD value and BEF

specified in table(3):

$$AGB(Mg/ha) = V \cdot WD \cdot BEF \tag{6}$$

Consequently the above ground biomass was obtained for the parcels selected:

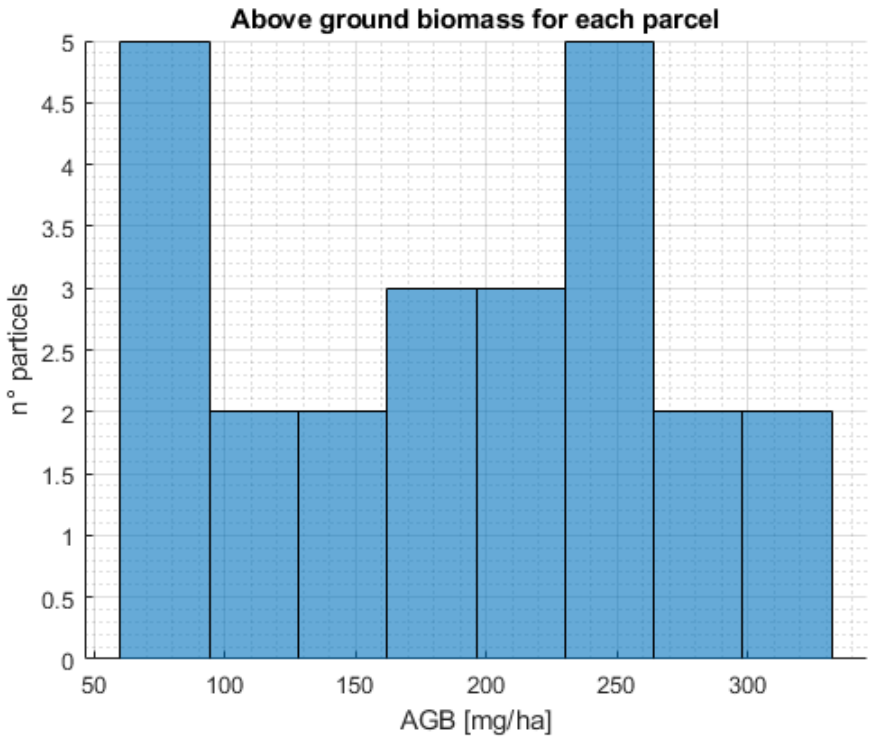


**Figure 9:** *Estimation of above ground biomass for each parcel*

As seen in the above figure the AGB for each polygon ranges from 63.9 Mg/ha (parcel 4) to 324.1 Mg/ha (parcel 7), its value depends on different factors such as vegetation type, density and cover but is mainly driven by the specific stock volume. It can be highlighted that the polygons with lowest and highest specific stock volume also have, respectively, lowest and highest AGB value.

### 3.6 PlanetScope dataset

The data set is obtained through the archive of the PlanetsScope missions. Each PlanetScope satellite is a CubeSat 3U form factor (10 cm by 10 cm by 30 cm). The complete PlanetScope constellation of approximately 130 satellites is able to image the entire land surface of the Earth every day (equating to a daily collection capacity of 200 million km²/day). This capacity changes based on the number of satellites in orbit and throughout the season, as satellites image less in the northern hemisphere in the winter time because of a decrease in the amount of hours with sunlight. PlanetScope images are approximately 3 meters per pixel resolution and have 8-bands, they are derived from the PSB.SD sensor (SuperDoves) [30]:

| | |
|---|---|
| Mission Characteristics | Sun-synchronous Orbit |
| Orbit Altitude | 475 - 525 km |

| | |
|---|---|
| Field of View | 4.0° (swath) 2.3° (scene length) |
| Frame Size | 32.5 km x 19.6 km |
| Revisit Time | Daily at nadir |
| Pixel Size | 3m |

**Table 4:** *Constellation overview*

### 3.7 PSB.SD instruments

The PSB.SD instruments consist of the next-generation "PSBlue" telescope with a larger 47 megapixel sensor and the same filter response as the previous technology (PS2.SD), in the Red, Green, Blue and NIR bands. The PSB.SD payloads extend this capability so that in addition to the four bands that are identical to the PS2.SD spectral bands (Red, Green, Blue, and NIR), there are four additional bands. These additional bands are Red Edge, Green I, Yellow, and Coastal Blue. Red Edge is meant to be interoperable with Sentinel-2 band 5. The framing of scene products obtained through PSB.SD are larger in both directions when compared to PS2.SD and Dove Classic scene products. Each frame consists of eight stripes, in order to generate the final 8-band image, a number of consecutive frames are stacked together on either side of a given frame.

| | |
|---|---|
| Coastal Blue | 431-452 nm |
| Blue | 465-515 nm |
| Green I | 513 - 549 nm |
| Green | 547 - 583 nm |
| Yellow | 600-620 nm |
| Red | 650 - 680 nm |
| Red-Edge | 697 - 713 nm |
| NIR | 845 - 885 nm |

**Table 5:** *Spectral bands*

### 3.8 PlanetScope calibration models

The atmospheric and geometric correction are applied to images, correcting sensor related effects using sensor telemetry and a sensor model. All PlanetScope satellite images are collected at a bit depth of 12 bits and stored on-board the satellites with a bit depth of up to 12 bits. Radiometric corrections are applied during ground processing and all images are scaled to a 16-bit dynamic range. This scaling converts the (relative) pixel DNs coming directly from the sensor into values directly related to absolute at-sensor radiances. The scaling factor is applied to minimize quantization error and the resultant single DN values correspond to 1/100th of a $W/(m^2 \cdot sr \cdot \mu m)$ [30]. The DNs of the PlanetScope image pixels represent the absolute calibrated radiance values for the image.

### 3.9 Atmospheric correction

Surface reflectance is determined from top of atmosphere (TOA) reflectance, calculated using coefficients supplied with the Planet Radiance product. The Planet Surface Reflectance product corrects for the effects of the Earth's atmosphere, accounting for the molecular composition and variation with altitude along with aerosol content. Combining the use of standard atmospheric models with the use of MODIS water vapor, ozone and aerosol data, this provides reliable and consistent surface reflectance scenes over Planet's varied constellation of satellites as part of the normal, on-demand data pipeline [30]. However, there are some limitations to the corrections performed, such as the absence in some instances of MODIS data overlapping a Planet scene or the area nearby, with the correction falling back to a predefined internal model. Stray light and adjacency effects are not corrected for also the effects of haze and thin cirrus clouds are not corrected for. Instead aerosol type is limited to a single, global model.

### 3.10 Radiometric preprocessing

The dataset is composed by 6 scenes, covering all the 24 parcels and mostly of the Alto-Adige region, the cloud coverage is less than 10% for elaboration purposes and the acquisition time is selected in order to capture vegetation in its flourishing period. Out of the 6 scenes selected, 5 are acquired on 10th September and the remaining on the 24th September. In the following figure the area captured by each acquisition is represented. The images are identified by their id number, which is shown inside the rectangle:

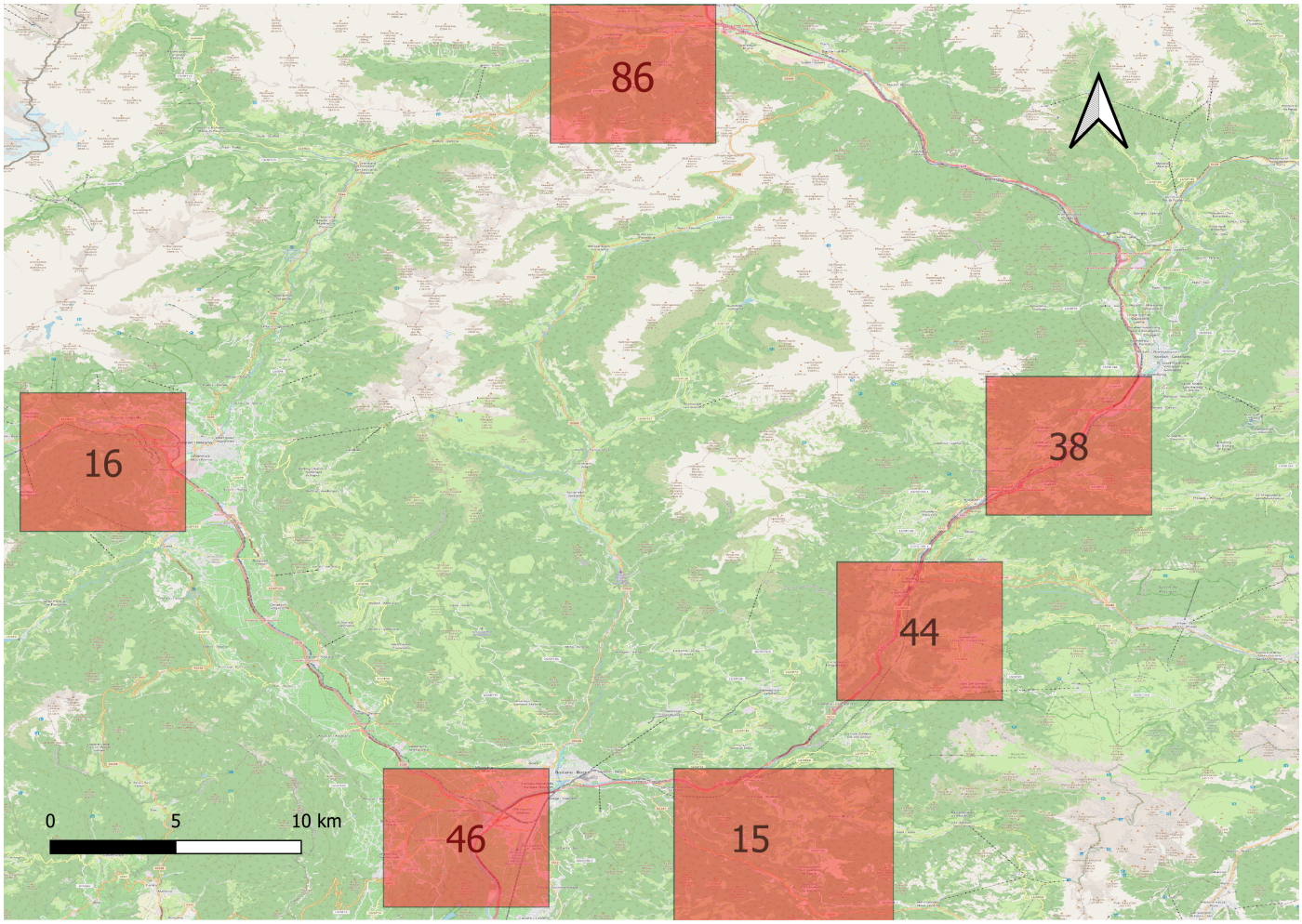


**Figure 10:** *Spatial reference of PlanetScope images*

All the acquisitions and the vector data are managed through the ENVI 5.7 software, PlanetScope data are imported as GeoTIFF files, instead vector data of the parcels are imported as shapefiles and then converted into ROIs. A detailed view of the study areas is obtained through PlanetScope images, they are paired with the regions of interest related to the polygons and presented in the next figures:


**Figure 11:** *Detail of scene 16*

Scene 16 captures the municipalities of Marlengo and Lagundo, the most common kind of vegetation in the area highlighted by the polygons is chestnut trees.


**Figure 12:** *Detail of scene 15*

Scene 15 contains Nova Ponente municipality and particle 262 is highlighted. The area contains mostly high vegetation and grassland with beech forests as the most common type.


**Figure 13:** *Detail of scene 38*

Scene 38 captures the municipalties of Velturno, Bressanone and Funes. The particles selected here fall mostly in the category of Norway spruce and temperate oaks.

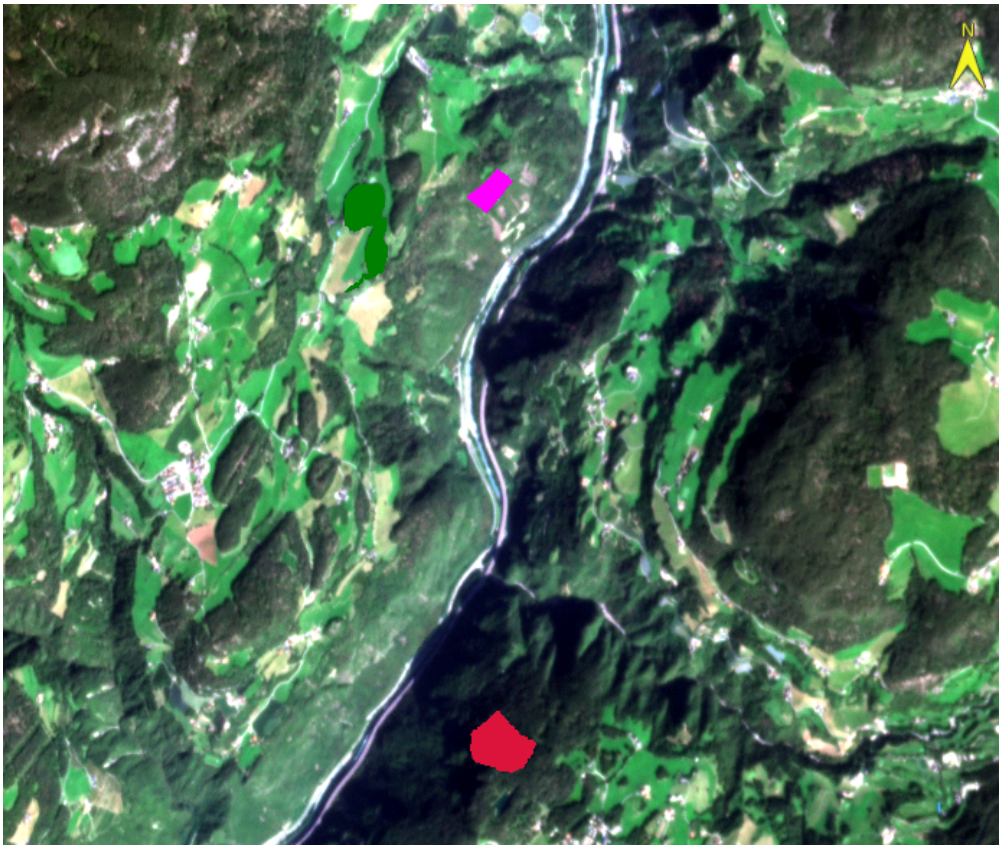


**Figure 14:** *Detail of scene 44*

Scene 44 captures the municipalities of Renon, Fiè allo Sciliar and Castellrotto. The forest species contained in the scene are scots pine and mountain pine forests together with hornbeam and hophornbeam forests.


**Figure 15:** *Detail of scene 46*

Scene 46 captures the city area of Bolzano with the municipalities of Stpos, Vadena, San Genesio, Appiano, Laives, Vanga, Bolzano, Dodiciville, Gries and Terlano with the polygons falling in the Laives area. The image contains a variety of land uses: a vast urban area, surrounded by crop fields, also the confluence between Isarco and Adige river can be seen in the area. The most common species of forest vegetation are beech forests and temperate oaks.

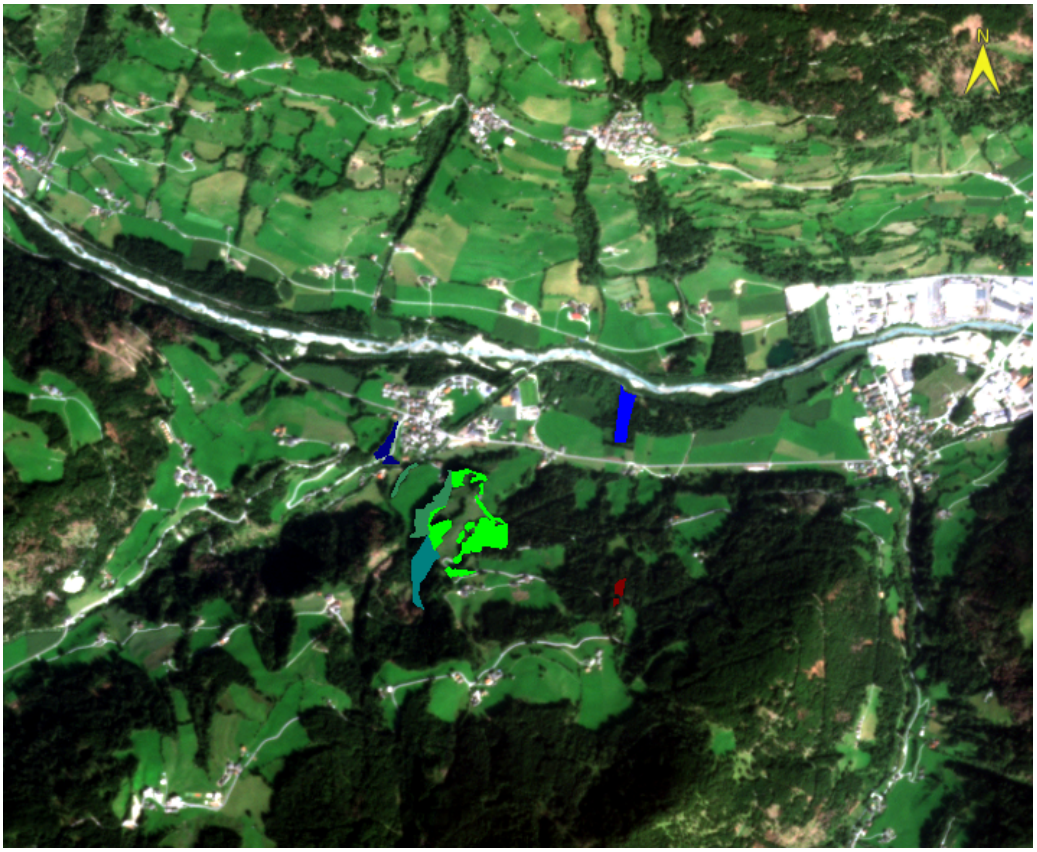


**Figure 16:** *Detail of scene 86*

Finally Scene 86 captures the municipalities of Vipiteno and Racines, the particles of this municipalities are populated almost entirely by Norway spruce forests. Before analyzing the data related to images a pre-elaboration of the scenes is operated. The radiometric calibration is applied to the images through ENVI's toolbox to convert the digital numbers recorded by satellite imaging systems into physical units. Those units are either radiance (W/m2/sr/µm) or apparent top-of-atmosphere reflectance, as for this purpose was preferred. The calibration was performed selecting for each polygon the corresponding ROI as the spatial subset, for example the result of the calibration for particle 262:

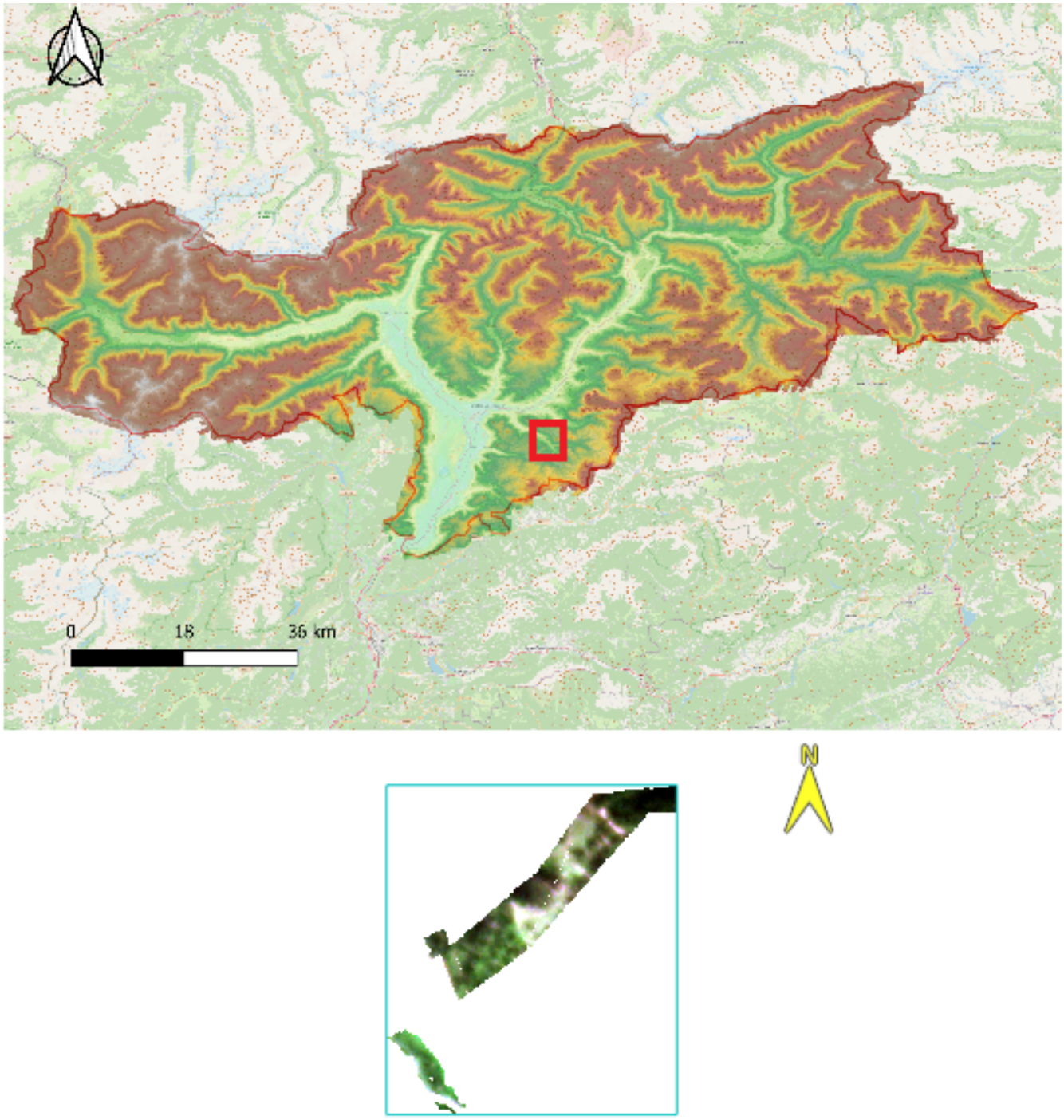


**Figure 17:** *Result of radiometric calibration for particle 262*

Relatively to particle 262, the following plot shows the mean with standard deviation, together with maximum and minimum value of DN:

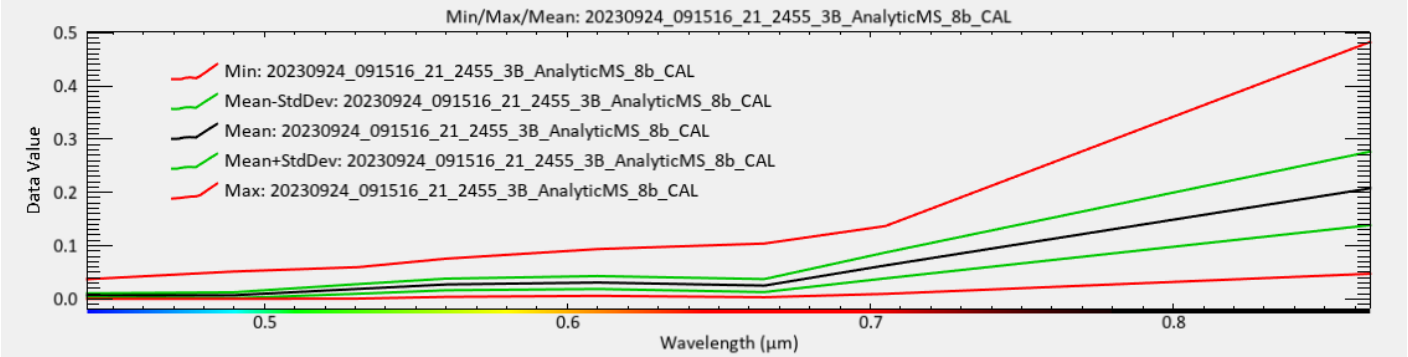


**Figure 18:** *Statistics of the calibration*

Also the histogram representing the distribution of the DN values for each band :

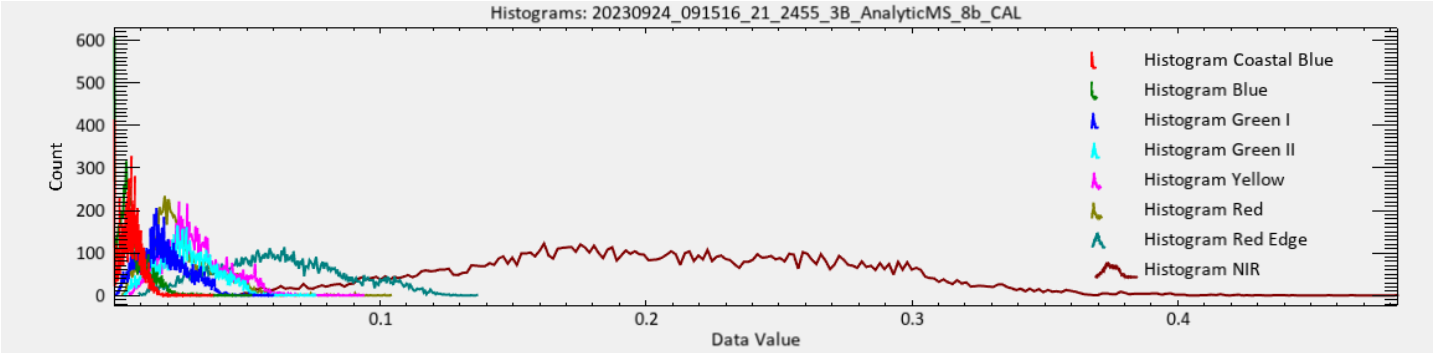


**Figure 19:** *Histogram distribution of calibrated images*

Eventually Dark Subtraction was applied to the images in order to exclude the effect of selective scattering from reflectance values. The operation assumes that some of the atmospheric effects such as scattering can be removed by finding the darkest pixels in an image and subtracting their values from all other pixels. The correction was applied to all of the 24 polygon but for illustrative purposes the results of the Dark Subtraction for particle 262 are highlighted in the following figure:

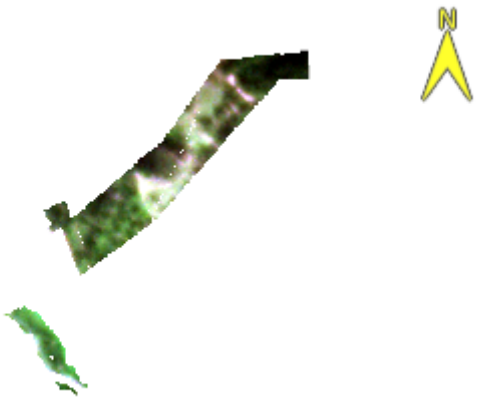


**Figure 20:** *Result of Dark Subtraction of particle 262*

To better visualise the vegetation components of the image, the false color representation will be

displayed. The image band associated with vegetation and its behavior, the NIR band, is assigned to the red visualization channel of ENVI, the red band associated to the green channel and blue band associated with blue channel, obtaining this results for scene 16(a) and scene 86(b):

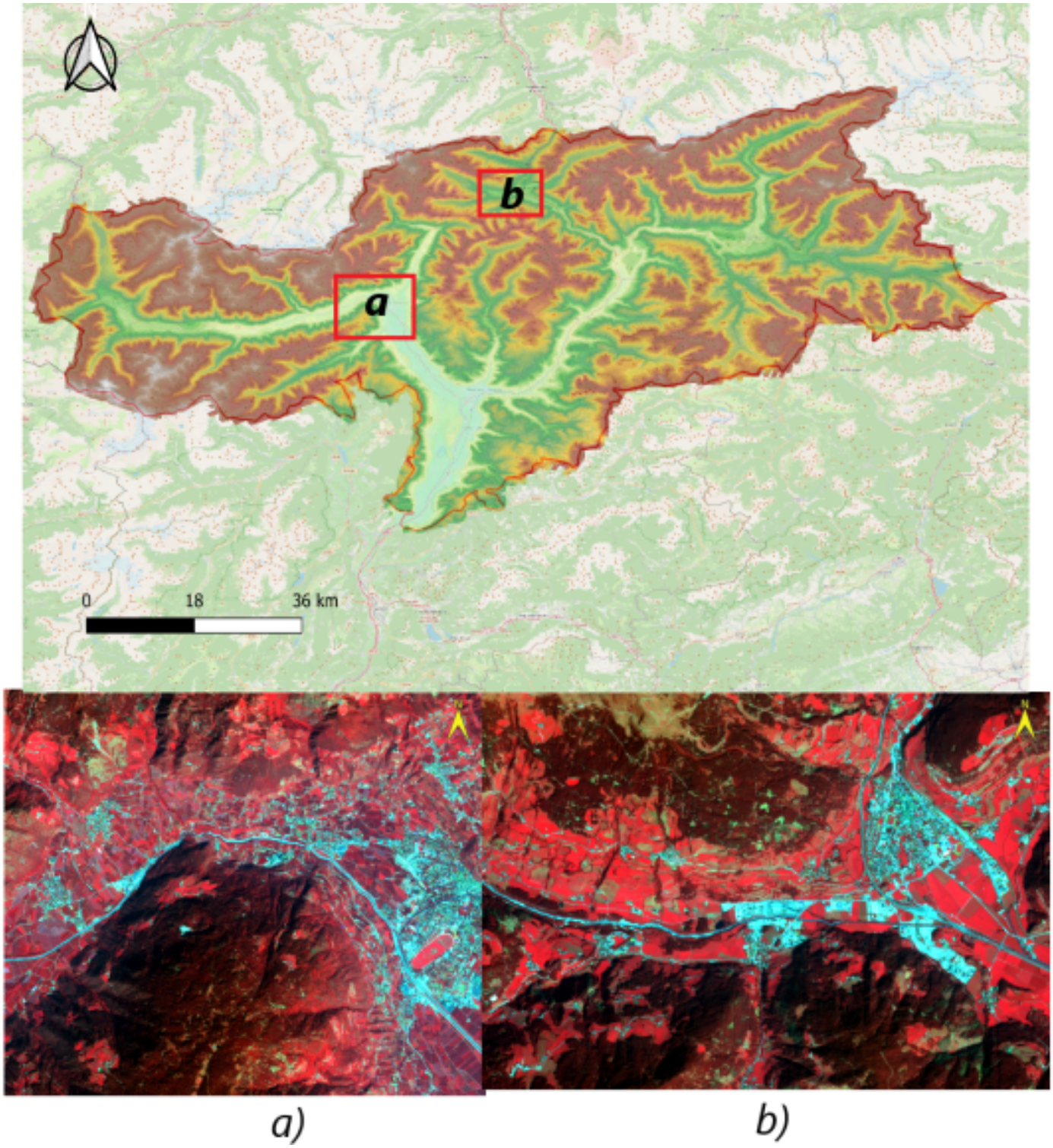


**Figure 21:** *False color representation for scene 16 (a) and 86 (b)*

The false color representation highlights vegetation areas with the red color as it can be seen from figure 21(a) and figure 21(b) being prevalent in the captured images. Urban areas such as the city center of Merano(a) and Vipiteno(b) are highlighted with cyan color.

### 3.11 Image classification

In the effort of characterizing areas captured by the scenes, calibrated and dark subtracted images were set to undergo a classification process, utilising the intrinsic function of ENVI software to perform an unsupervised classification through the ISODATA algorithm. Selecting the expected number of classes, at least equal to 5 and at maximum equal to 10 and the number of iterations to be performed equal to 10, the operation was carried out for all the scenes, for instance the following pseudo-color image is obtained for scene 16:

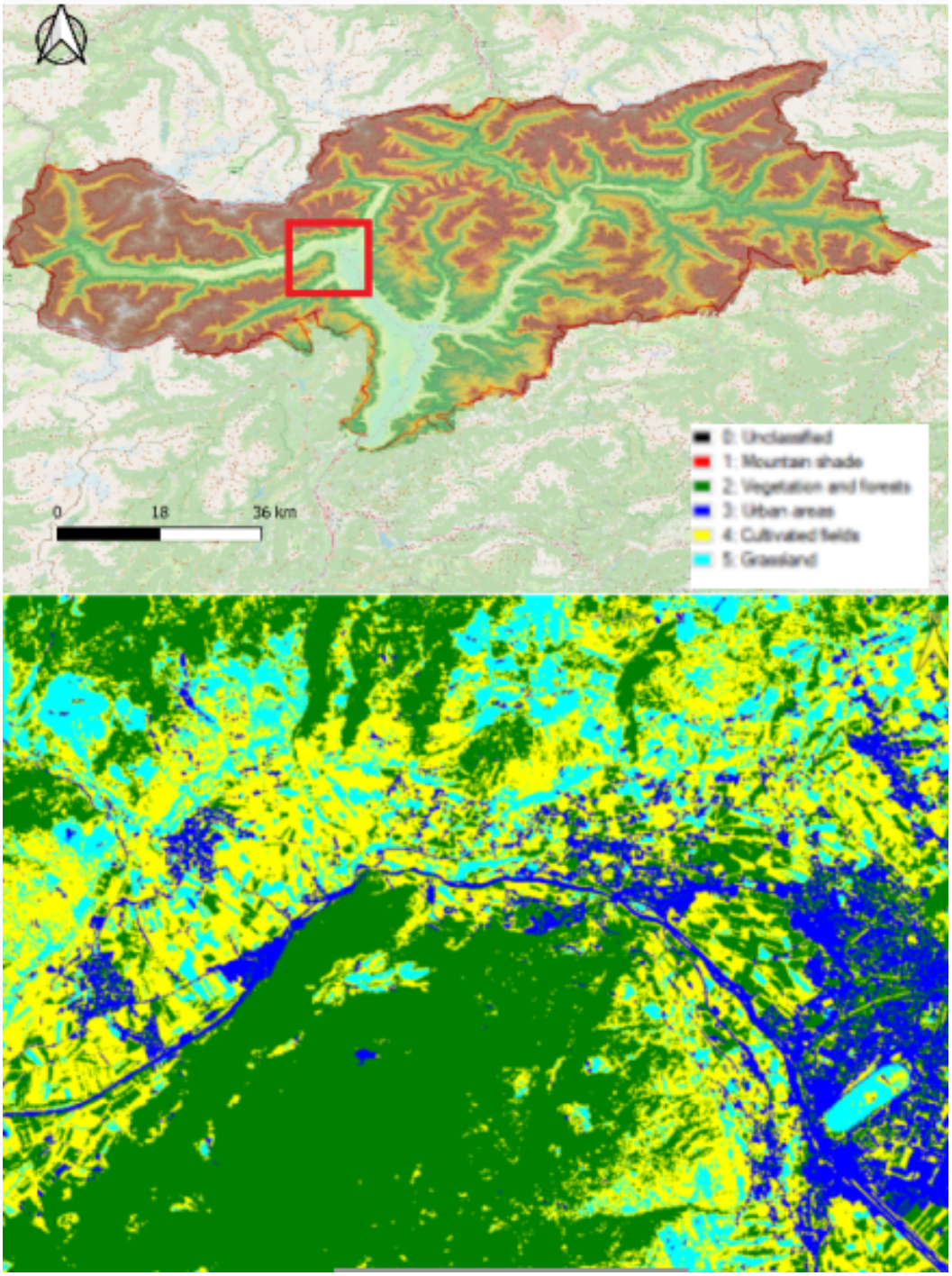


**Figure 22:** *ISODATA classification for scene 16*

| Class | Scene percentage [%] | Acc Pct [%] |
|---|---|---|
| Mountain shade | 0 | 21.5 |
| Vegetation and forests | 45.4 | 45.4 |
| Urban areas | 9.6 | 55.0 |
| Cultivated fields | 33.2 | 88.2 |
| Grassland | 11.8 | 100 |

**Table 6:** *Results of ISODATA classification for scene 16*

The classified image shows the area surrounding the city of Merano in he north-west part of the region. Identified as class 3 the city center and the infrastructures related are represented through the blue color. Cyan color identifies the grassland and fields, yellow class contains mostly apple crops and cultivated areas. Isodata algorithm classifies inaccurately shady parts of mountains as a seprate class, through *Band Math* function of ENVI the pixels falling in this category are assigned to their proper class. The most widely represented area, with 45.4% of pixels, is high vegetation and forests which covers the mountain sides above the city and in which the polygons are situated.

# 4 Results

In this section the results of the study will be summarized. For each of the particles, the calibrated and corrected acquisition will be analyzed through ENVI's tool *Spectral Indices*. The indices selected for the research are the GCI(Green Chlorophyll index), EVI(Enhanced Vegetation index), GNDVI(Green Normalised Difference Vegetation index), LAI(Leaf Area index) and NDVI(Normalised Difference Vegetation index), they will be generated for all the 24 study areas and their statistics computed:

| Index | Mean | Range | Median | First quartile | Third quartile | Std Dev. |
|---|---|---|---|---|---|---|
| EVI | 0.37 | 0.22-0.55 | 0.35 | 0.30 | 0.44 | 0.1 |
| GCI | 5.86 | 3.86-7.56 | 5.77 | 5.26 | 6.46 | 0.90 |
| GNDVI | 0.74 | 0.64-0.79 | 0.74 | 0.72 | 0.76 | 0.03 |
| LAI | 1.24 | 0.67-1.88 | 1.14 | 0.96 | 1.47 | 0.36 |
| NDVI | 0.80 | 0.73-0.83 | 0.80 | 0.79 | 0.82 | 0.02 |

**Table 7:** *Statistics of index generation from the 24 polygons*

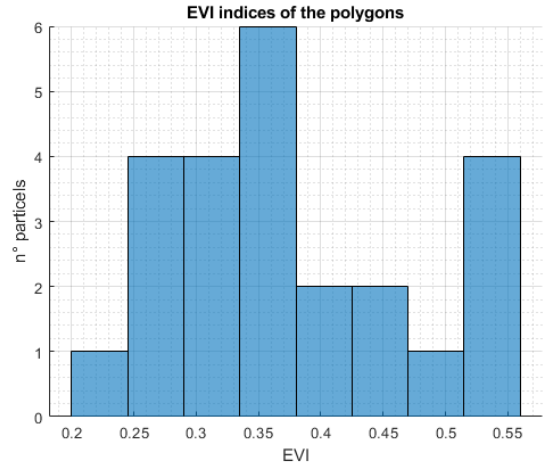


**(a)** *distribution of EVI index values*

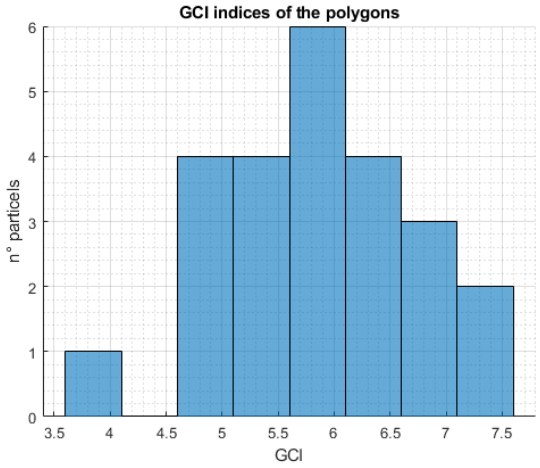


**(b)** *distribution of GCI index values*

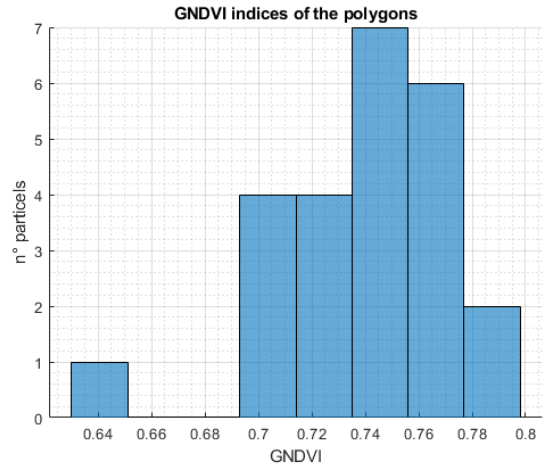


**(c)** *distribution of GNDVI index values*

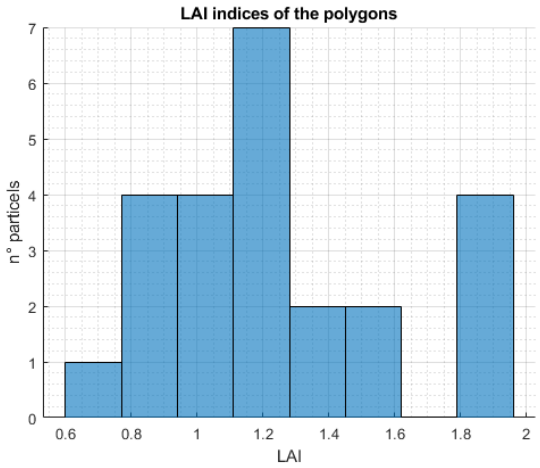


**(d)** *distribution of LAI index values*

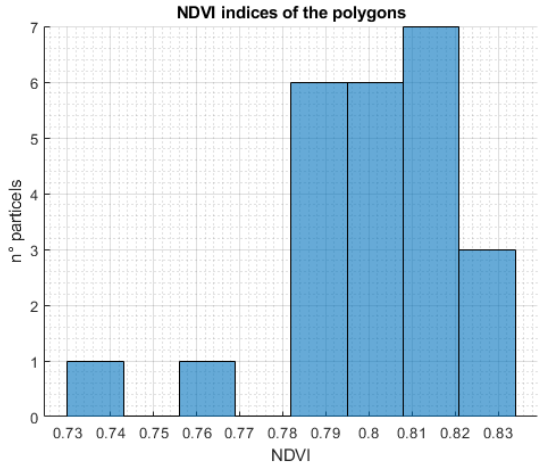


**(e)** *distribution of NDVI index values*

**Figure 23:** *Histograms of indices values*

Figures 23(a) to 23(e) show the values for each index among the 24 particles: GCI values appear to be scattered with strong variability between 3.8 and 7.5, actually they are characterized by the highest standard deviation of all dataset; LAI index also has high standard deviation among the polygons, which can be explained considering the different vegetation species captured, having a variety of leaf areas. The

other indices (EVI, NDVI, GNDVI) have relatively small variation in their values, being accompanied by a limited value of standard deviation. The similar meaning of NDVI and GNDVI indices is shown in their trend, which is very much related, being GNDVI a derivation of NDVI that uses the green band instead of the red band.

The values of each index will be now analyzed separately in order to highlight any possible trend. At this point the particles are divided into two groups: one group used for the calibration of the model through measured stock volumes data and the other for quantifying the accuracy of the model's estimation, since field data are available for the second group as well. The quality of the estimation is evaluated with the Root Mean Square Error, it uses true measurements at each predicted data point and is expressed through:

$$RMSE = \sqrt{\frac{\sum_1^N |y(i) - y'(i)|^2}{N}} \tag{7}$$

where N is the number of data points, y(i) is the i-th measurement, and y'(i) is its corresponding prediction. For calibration phase particles of different municipalities are selected with particular attention to excluding outliers data. Of the polygons selected for the model's calibration, the mean index values and stock volume will be interpolated in order to find a relationship that would forecast the stock volume in the remaining particles. The efficiency of the fit will be evaluated with $R^2$ coefficient, called coefficient of determination, $R^2$ measures how well a statistical model predicts an outcome. The outcome is represented by the model's dependent variable, in this case the stock volume. The lowest possible value is 0 and the highest possible value is 1, indicating a perfect interpolation.

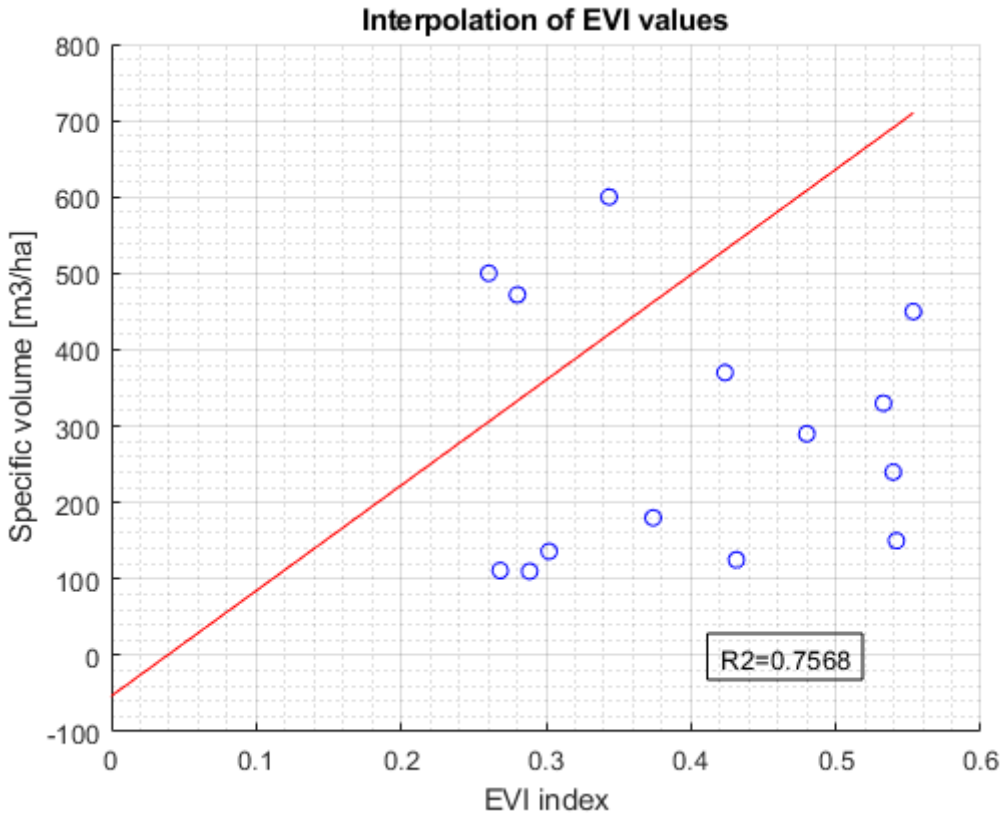


**Figure 24:** *Interpolation of EVI values*

The interpretation of EVI values depends on the specific ecosystem analyzed and local conditions, a value considered high for arid environment with scarce vegetation might be considered very low instead for rain-forest. Most of the index values fall in the range of 0.2-0.4 suggesting moderate vegetation presence with good health and active cover. As it can be seen in figure 24, the points representing 11 polygons align themselves with good results on the interpolation line with equation:

$$V = -53.3160 + 1.3790e + 03 \cdot EVI \tag{8}$$

For the model, $R^2$ coefficient results in a value close to 0.76, suggesting that EVI index variation could explains the variation in stock volume in the surfaces. Considering $R^2$ coefficient, EVI can approximately follow the variation of stock volume but cannot describe with precision the small nuances and its changes.

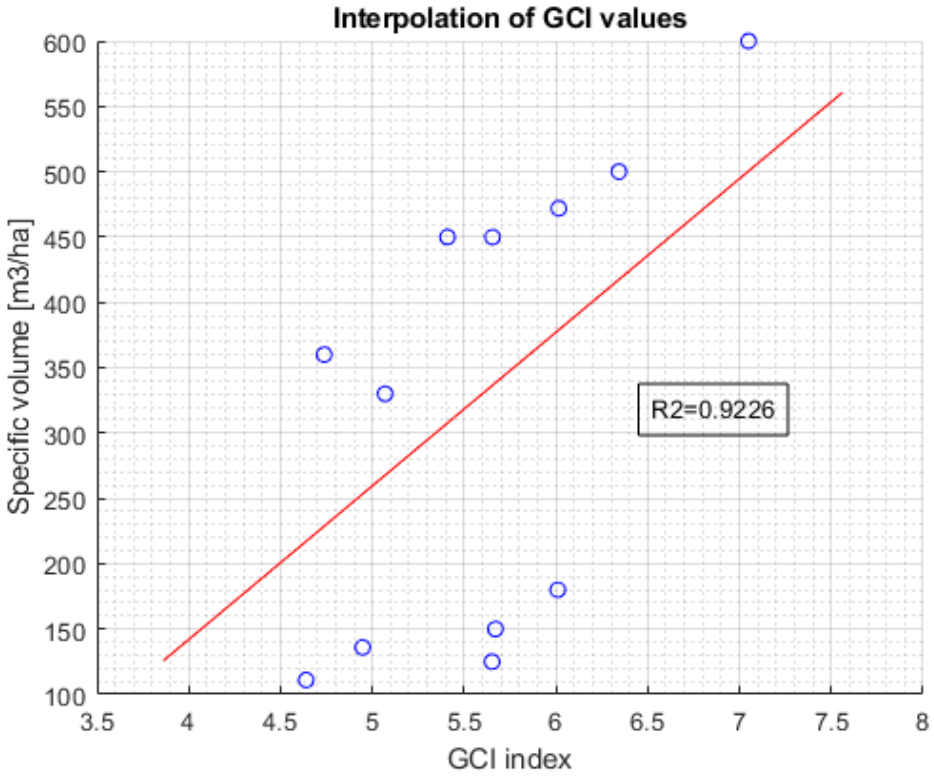


**Figure 25:** *Interpolation of GCI values*

Also the interpretation of GCI values requires the knowledge of local conditions and vegetation types, for instance some species might have naturally a higher values respect to others, moreover other factors such as sensor technology and illumination conditions at the acquisition have an important role. Generally a GCI value between 4-5 is considered high and points to a strong presence of Chlorophyll in the study areas, which suggests a good health of vegetation. GCI index has the highest standard deviation of all the indices, the minimum value recorded is 3.86, which demonstrate the high Chlorophyll content for the species selected in this period of the year, maximum value of GCI is 7.56, considered very high. For this preliminary analysis a high GCI mean value of 5.86 indicates that leaves are in healthy state with high photosynthetic activity.

The results of model's calibration using GCI index are highlighted in figure 25. For the polygons selected the points representing index values and stock volumes are displayed in the plot, together with the red interpolation line with equation:

$$V = -328.2214 + 117.5562 \cdot GCI \tag{9}$$

The model obtained has a very high value of $R^2$ coefficient, indicating that GCI might be the most effective indicator in the stock volume estimation.

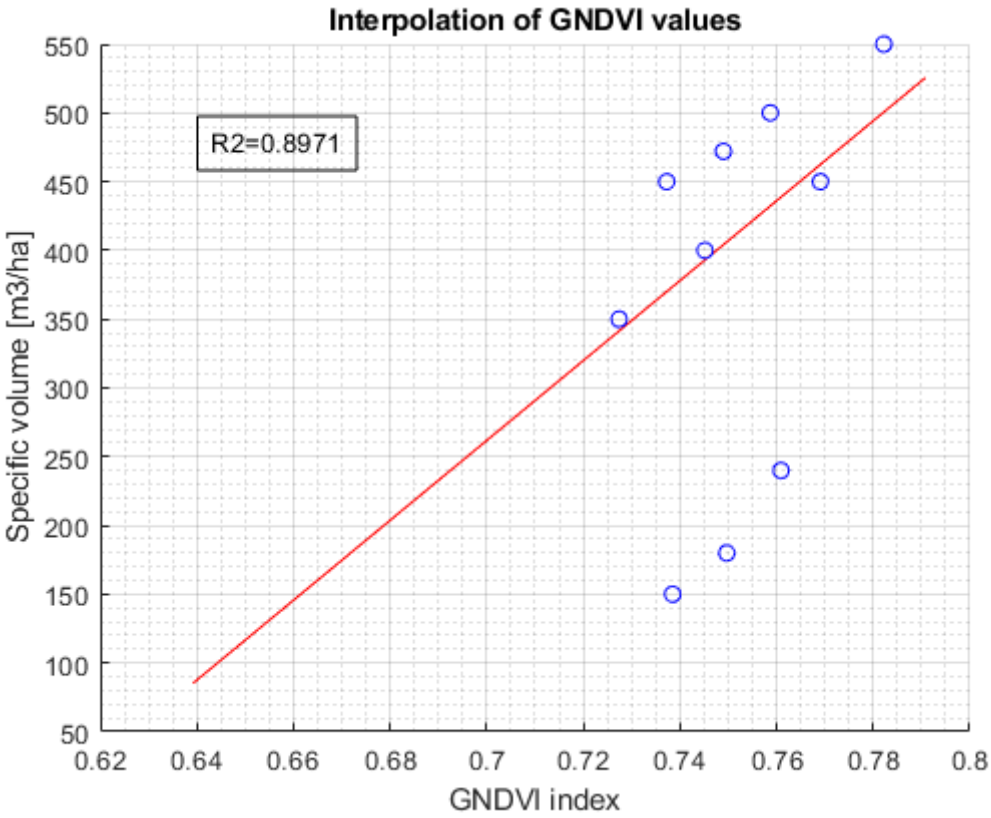


**Figure 26:** *Interpolation of GNDVI values*

GNDVI is similar to NDVI but utilises the green and NIR bands to assess the vigor and vitality of vegetation. As for other indices a deep interpretation of GNDVI values takes into account local conditions and species, soil conditions and seasonality. A value of 0.7 is typical of good health and strong vitality of vegetation:

- Vitality: GNDVI values ranges from -1 to 1 so a value of 0.7 is considered high, indicating that vegetation in study area is in good health and with strong photosynthetic activity
- Leaves cover: GNDVI is sensitive to chlorophyll content and density of leaves cover. Mean value of 0.7 is associated with a dense leaves cover and high concentration of chlorophyll, all symptoms of healthy vegetation.

The interpolation of stock volume using GNDVI index results in the plot obtained in figure 26, where the points for the polygons selected are represented with the line that interpolates them:

$$V = -1.7713e+03 + 2.9044e+03 \cdot GNDVI \tag{10}$$

The trend of the line shows that higher values of the index, correspond to a higher value of the stock volume, just as it is expected. The good result of the regression is confirmed by the $R^2$ coefficient, close to 0.9, indicating that also GNDVI index could be used in this environment to forecast stock volume variations.

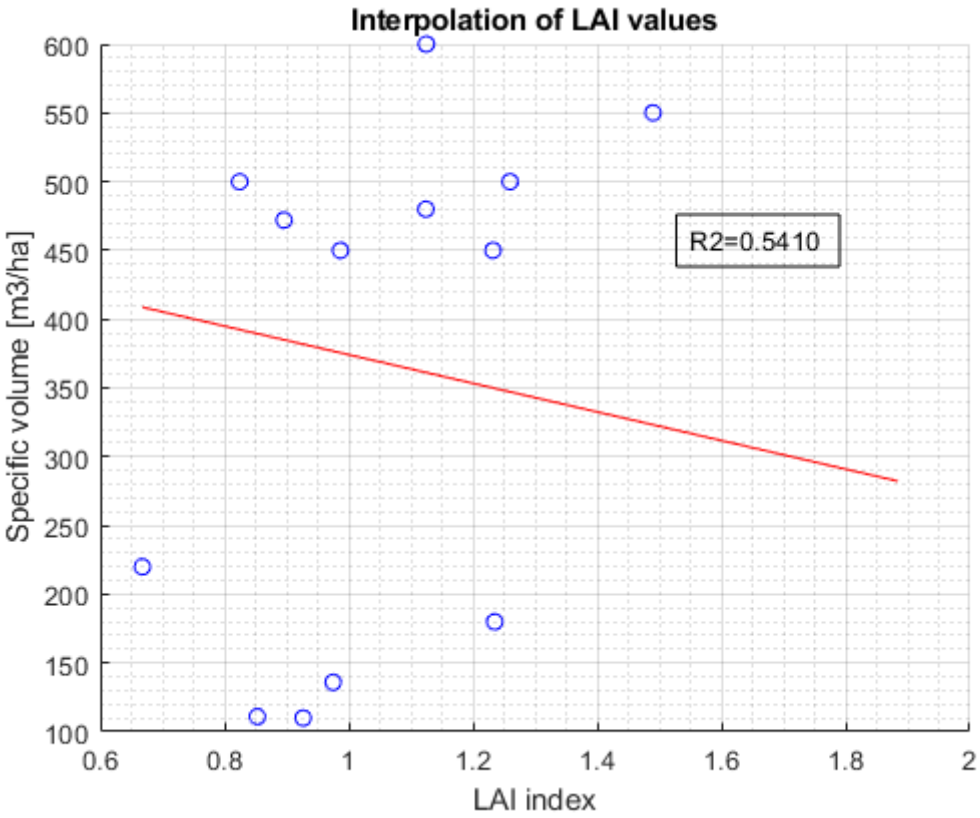


**Figure 27:** *Interpolation of LAI values*

Leaf Area Index (LAI) is a key parameter in ecology and in the management of natural resources because it measures the ratio between the leaf area and the area of the underlying soil. LAI index is used also to quantify ecological variables such as light interception, photosynthetic activity and water cycle of plants. A low value of LAI index suggests a lower photosynthetic capacity and a lower gaseous interchange with the atmosphere. The mean value of 1.24 is considered medium to low with the presence of a shallow vegetation cover or moderate leaf density:

- Leaf density: the LAI mean value indicates that for each square meter of soil captured a leaf area of 1.24 square meter is measured. This is the case of scarce vegetation but considering local species and conditions, most probably is related to the small surface of the leaves of the most common species observed, which for evergreen trees resemble the needle-like shape.
- Seasonality and species: two factor that greatly influence the LAI value. A low value is typical of deciduous species during winter season, so the LAI value in the study areas can be affected also by the approaching of cold season, which in this alpine climate already manifests itself by end of September, when images were acquired.

The regression model obtained utilising LAI index is shown in figure 27: for the polygons selected, the points align well along the interpolation line with equation:

$$V = 478.1704 - 103.9920 \cdot LAI \tag{11}$$

The points are quite scattered and so their trend cannot be described well by the regression model, this result is also confirmed by the $R^2$ coefficient, which is lower than 0.6, suggesting that the LAI index is not appropriate for the estimation, considering the local condition of the study areas and the species selected.

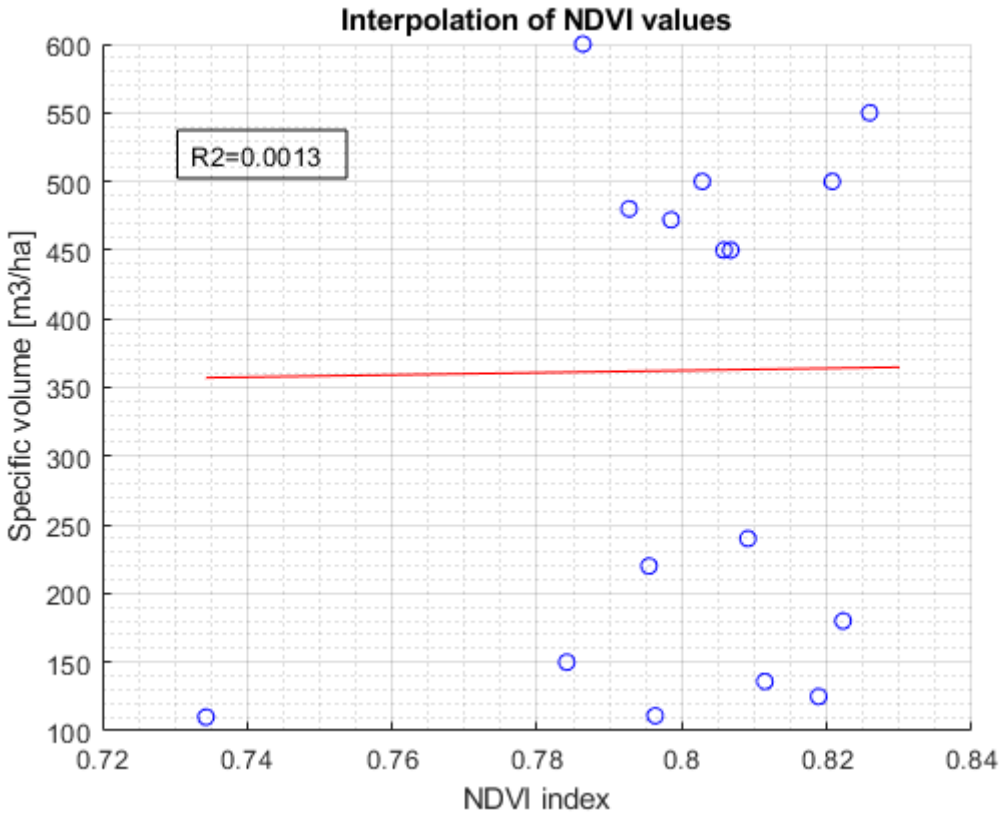


**Figure 28:** *Interpolation of NDVI values*

Finally coming to the last index considered, NDVI. From table 7, the small range of variation of NDVI index is highlighted, with a mean value of 0.8, in accordance with the values recorded for these ecosystems. Values higher than 0.6 are related to dense green vegetation surfaces.

The points represented in figure 28 are sparse and the interpolation line cannot describe the variation of the stock volume. The regression line has the following equation:

$$V = 298.3684 + 79.9810 \cdot NDVI \tag{12}$$

The value of $R^2$ coefficient close to 0 confirms the inappropriateness of the model in describing the fluctuation of stock volume. NDVI is frequently related with herbaceous or total green biomass (tons/ha) for given vegetation types and photosynthetic activity, but for the local environment considered in this study other indices demonstrate a higher correlation to stock volume. More specific indices derived from NDVI, such as GNDVI index, could be helpful in the description of environmental variables.

| Index | $R^2$ | a | b |
|---|---|---|---|
| EVI | 0.7568 | -53.3160 | 1.3790 e+03 |
| GCI | 0.9226 | -328.2214 | 117.5562 |
| GNDVI | 0.8971 | -1.7713 e+03 | 2.9044 e+03 |
| LAI | 0.5410 | 478.1704 | -103.9920 |
| NDVI | 0.0013 | 298.3684 | 79.9810 |

**Table 8:** *Regression parameters and coefficient of determination* $R^2$

## 4.1 Stock volume prediction

The final part of this study aims to predict the stock volume contained in the second group of polygons, using the coefficient reported in table 8, the regression models will be applied. Since the effective stock volume data of the second group of particles is also available through the forest sheets, the accuracy of the forecast can be evaluated.

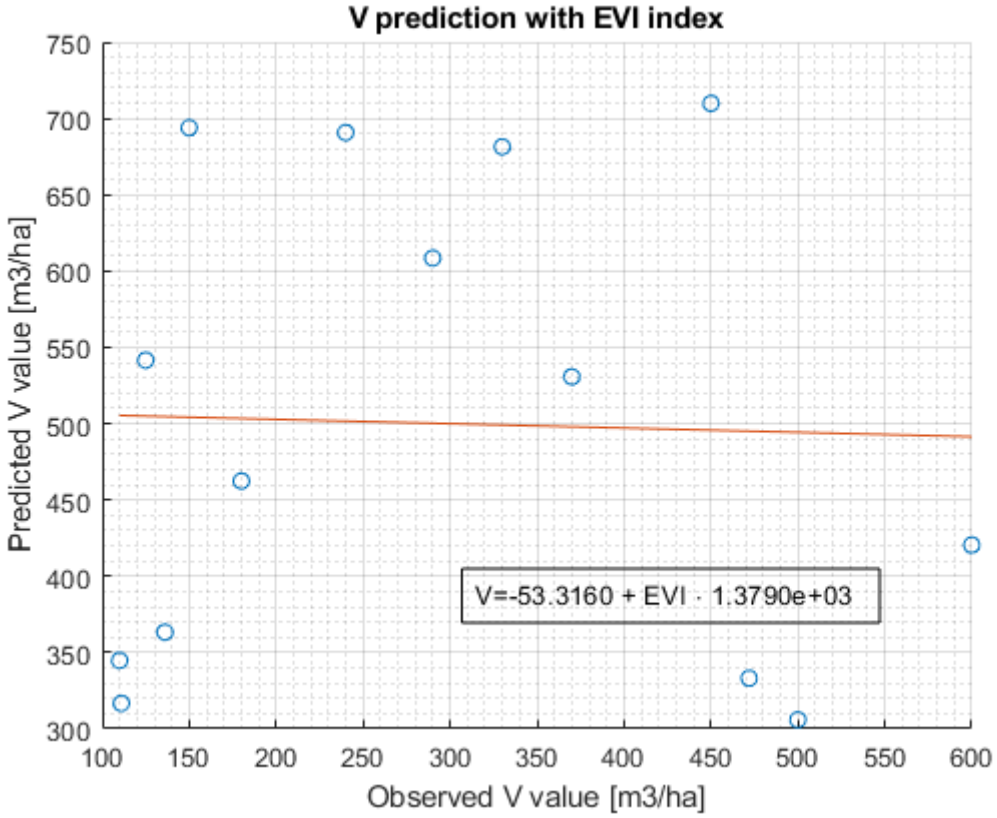


**Figure 29:** *Prediction of stock volume data though EVI index*

The results are displayed in plots such as the one in figure 29, on the horizontal axis the observed stock volume data contained in the sheets is reported, instead on the vertical axis the stock volume predicted through the regression model is represented. The regression model is implemented by extracting the mean EVI index value of all the cells of the polygon through ENVI's tool and applying equation 8 to obtain the forecast. Figure 29 shows the coordinates of the points obtained though the application of

the model used for prediction and the line that interpolates them. Ideally the points should align along a diagonal line with equation y=x.

The regression model obtained using GCI index is applied to obtain the stock volume prediction:

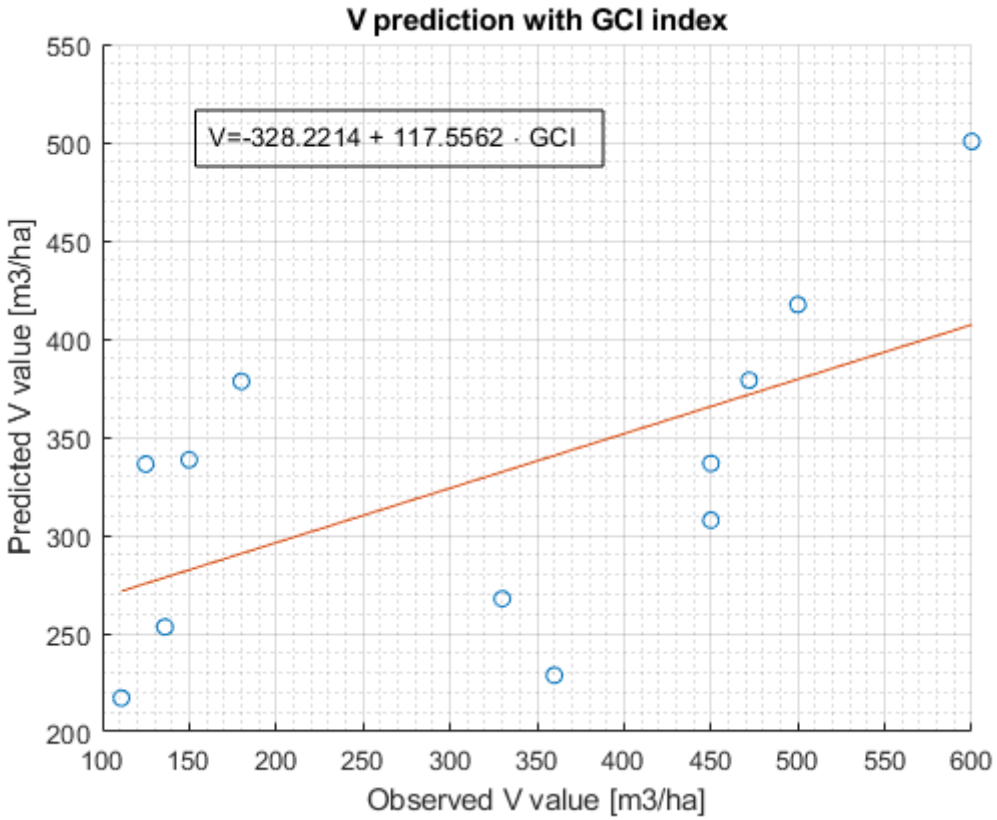


**Figure 30:** *Prediction of stock volume data though GCI index*

Figure 30 highlights the results of the application of equation 9 compared to the actual values recorded in the sheets for the second group of particles. Considering $R^2$ value of table 8 for GCI model, prediction process is expected to give precise results. The high number of polygons with a stock volume in the range of 300-500$m^3/ha$ allows the model to be calibrated having a high reliability in this interval. The predicted points align well along the red line with the highest coefficient of determination of all models, suggesting GCI index could be the best estimator of volume and biomass in this environment.

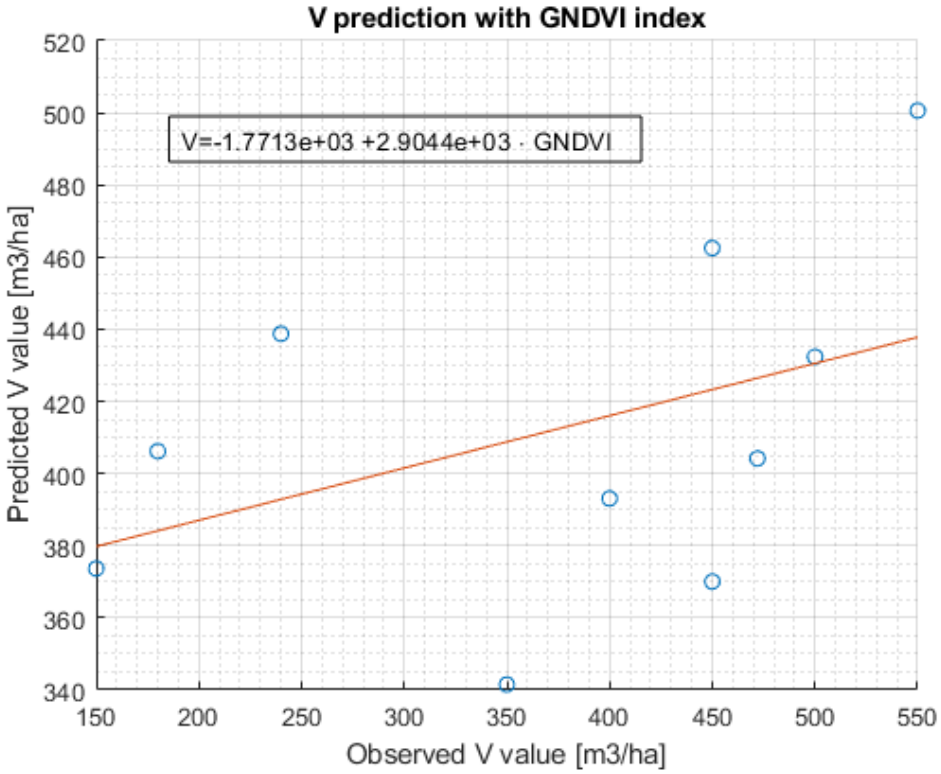


**(a)** *Prediction of stock volume data though GNDVI index*

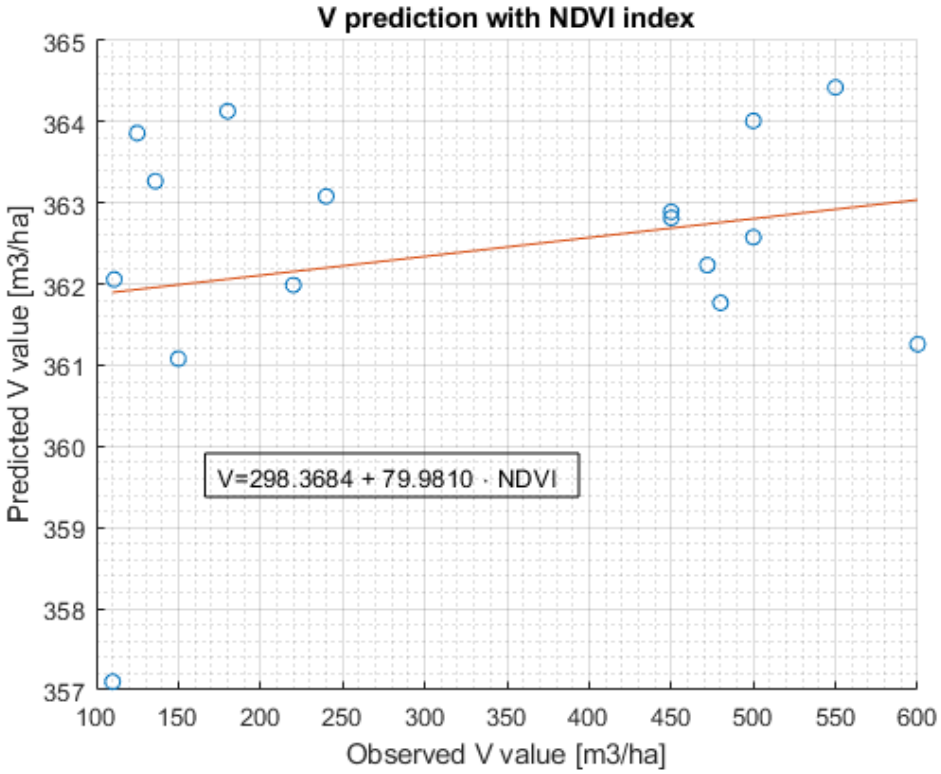


**(b)** *Prediction of stock volume data though NDVI index*

**Figure 31:** *Volume prediction through GNDVI and NDVI index models*

Figures 31(a) and 31(b) show respectively the stock volume prediction results using the models calibrated with GNDVI index and NDVI index. To predict the data, the models are implemented through

equation 10 (GNDVI) and equation 12 (NDVI), parameters and determination coefficients reported in table 8 characterise the models. Previous section already discussed the inappropriateness of NDVI index in describing the natural fluctuation in biomass quantity of the particles considered, the result is confirmed once again from figure 31(b): the prediction points are not aligned over the interpolation line with a $R^2$ very low and especially for low stock volumes the estimation appear to be very imprecise. Figure 31(a) shows how a more specific index (GNDVI) could be more sensitive into representing the natural variation of biomass on each surface, application of GNDVI model shows a very good results in the forecast phase, making it eligible for one of the best predictors of the set.

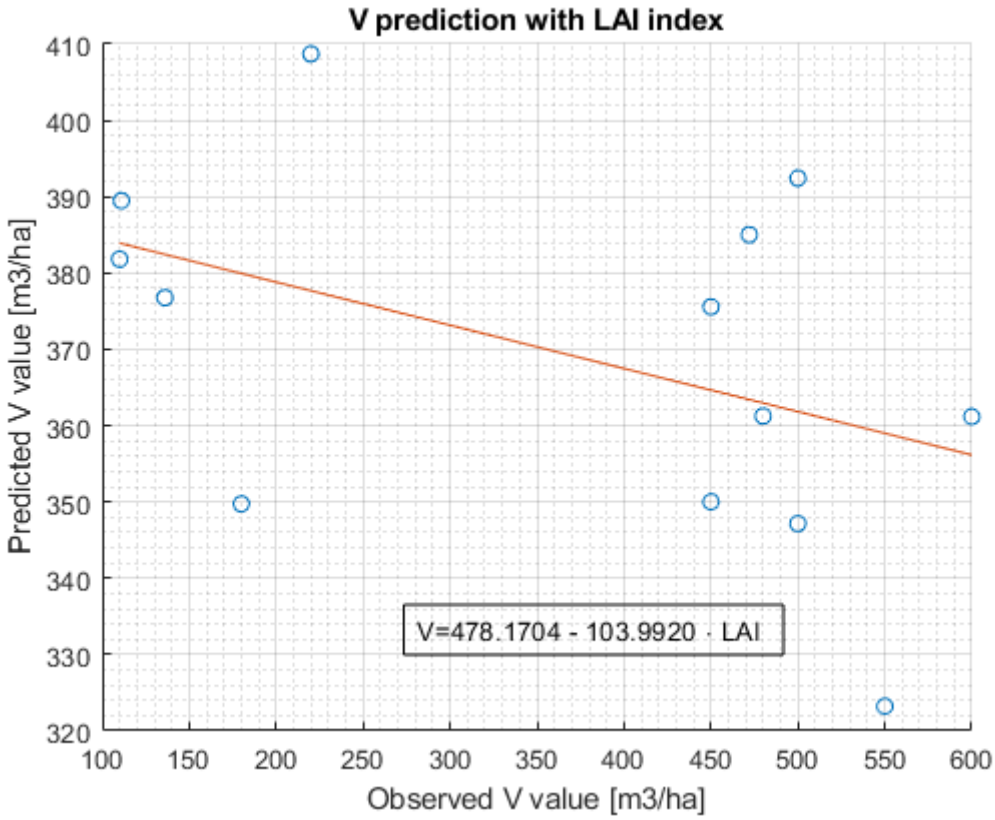


**Figure 32:** *Prediction of stock volume data though LAI index*

Finally figure 32 shows the results of the application of the model calibrated using LAI index. For the prediction, equation 11 is applied and the points are displayed on the plot relatively to their observed value. From the characteristics of the model reported in table 8, prediction process is not expected to give precise results. In fact, it is clear from figure 32 the scattering of the points on the plot, the model is not able to reproduce or predict any real values of biomass.

| Index | RMSE [m3] |
|---|---|
| EVI | 305.75 |
| GCI | 136.67 |
| GNDVI | 126.08 |
| LAI | 186.96 |

| NDVI | 179.69 |
|---|---|

**Table 9:** *Results of volume prediction process*

Considering the prediction results in table 9 and the models' quality assessed in table 8 through $R^2$ coefficient, GCI and GNDVI are selected to be the most reliable indices for estimating the biomass of the area. The main parameter that affects biomass presence is the stock volume and considering the accurateness by which these indices predict it, leads to believe that they will be suited also for biomass prediction.

## 4.2 Results' mapping

To better understand the context of the results of previous section the data are mapped considering the already analyzed particle 262 as the example area. The file generated by ENVI's tool *Spectral indices* contains for every pixel of the polygon the value of the selected index, which can be converted through a simple *Band math* operation into stock volume using equations 8-12. For particle 262 the related region of interest falls inside the red contours and is represented here over PlanetScope scene 15:

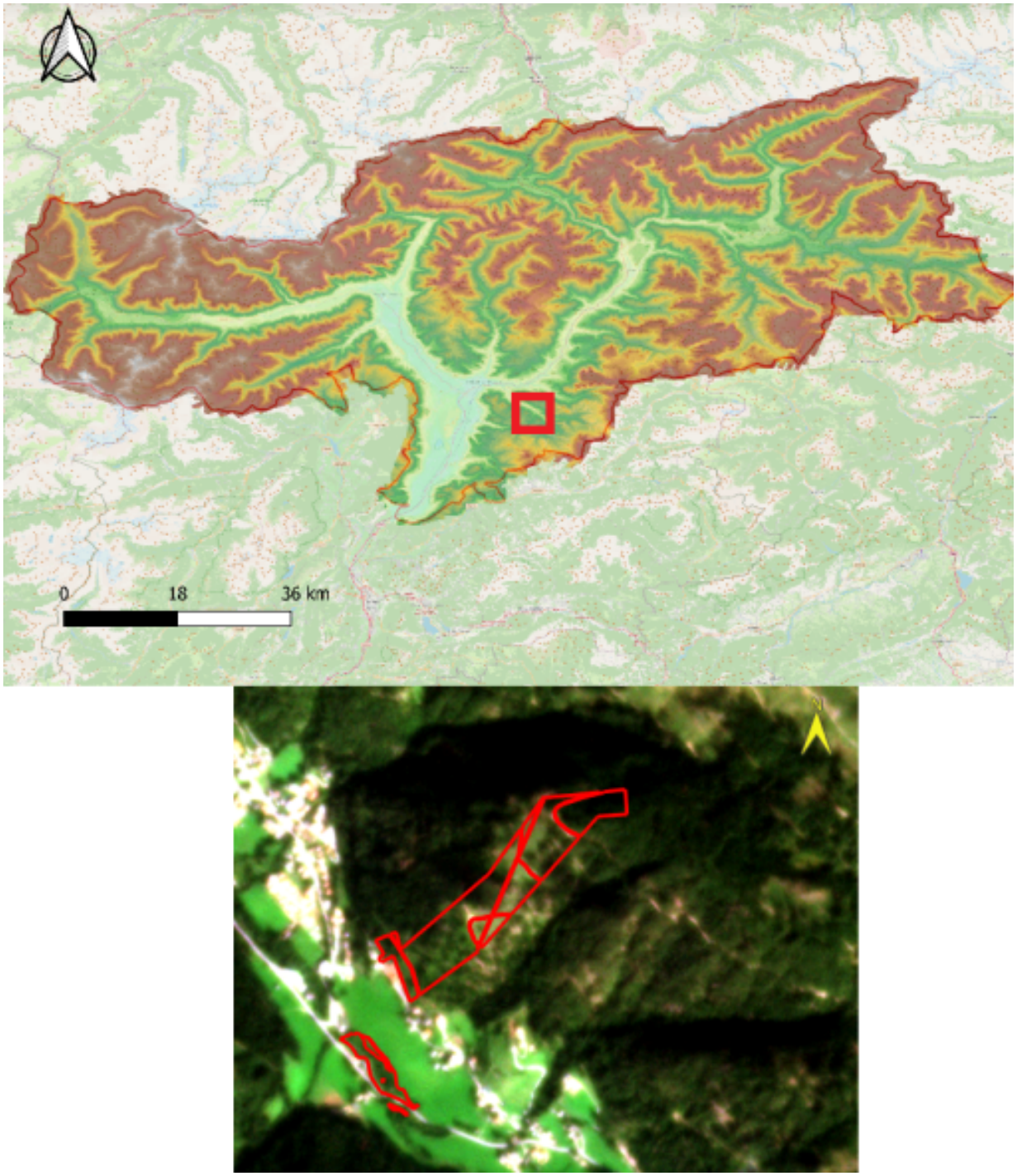


**Figure 33:** *Contours of particle 262*

The area falling inside the polygon is a sloping forest made up mostly of Norway spruce (69%) Scots pine (20%) and white fir(10%) with the presence in small quantity of larch(1%). The area corresponds to the particle with the highest stock volume and the highest value of above ground biomass of the dataset, respectively 5682 $m^3$ and 324 mg/ha.

Considering the results of table 9, GCI and GNDVI are the indices that can best describe the difference in stock volume of a particular area. Through a color scale ranging from low values in blue and high values in red, the GCI and GNDVI index values are mapped:

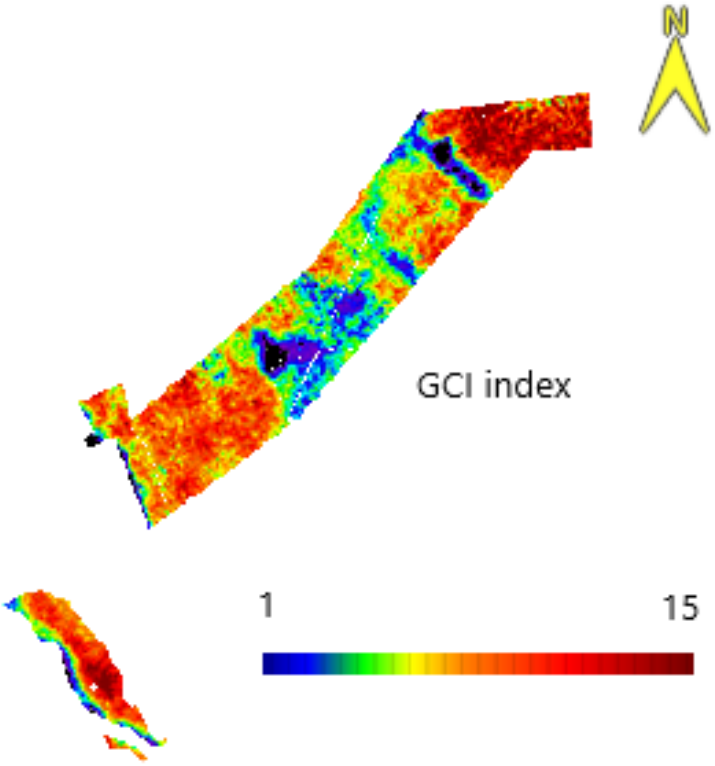


**(a)** *GCI index values map of particle 262*

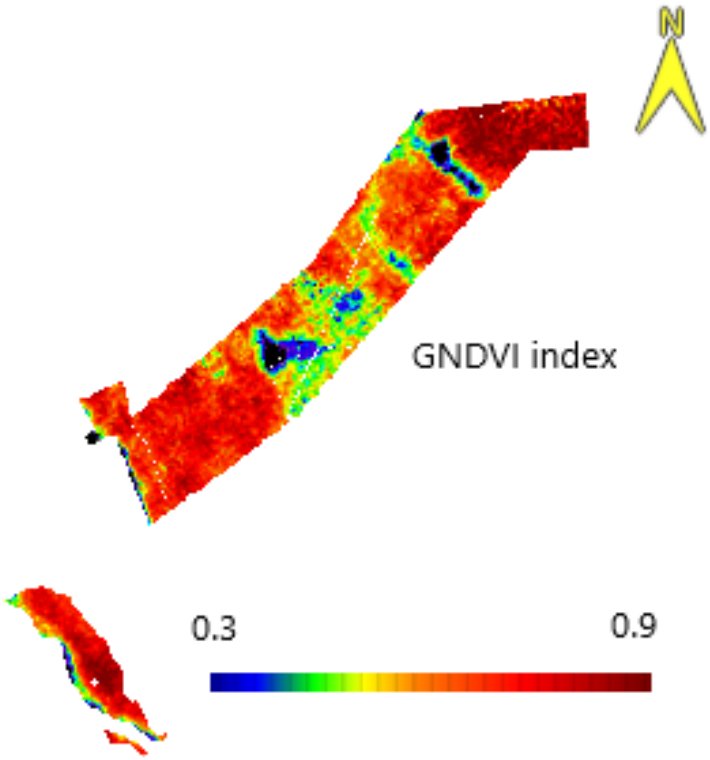


**(b)** *GNDVI index values map of particle 262*

**Figure 34:** *Indices distribution over particle 262*

Eventually applying equation 9 and equation 10 through ENVI's band math the spatial distribution of the stock volume can be obtained for particle 262:

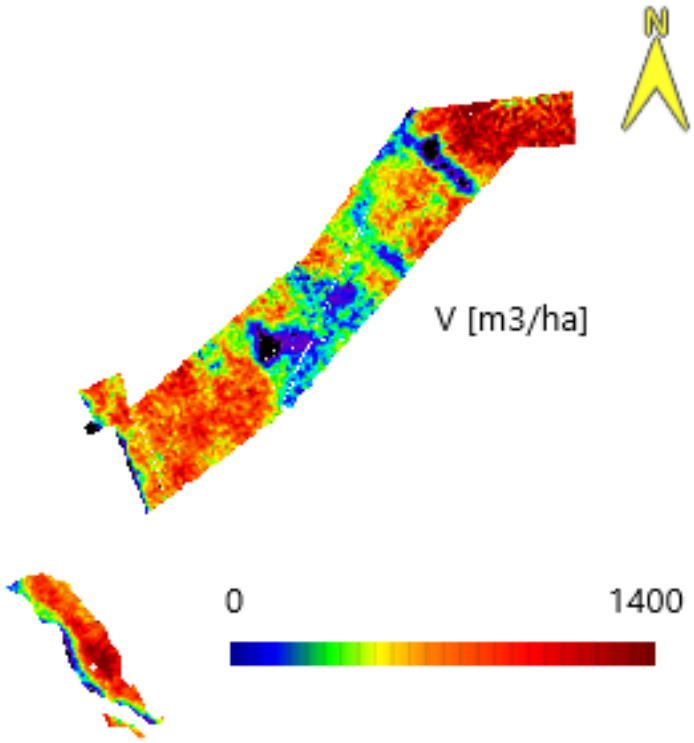


**(a)** *Spatial distribution of stock volume for particle 262 through GCI index*

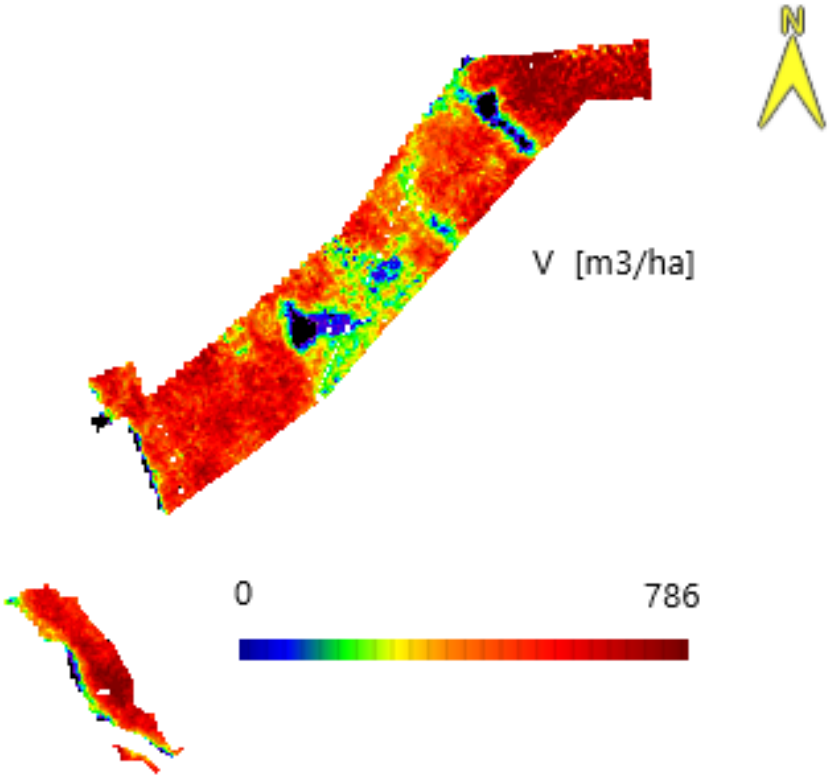


**(b)** *Spatial distribution of stock volume for particle 262 through GNDVI index*

**Figure 35:** *Volume distribution over particle 262*

The high biomass quantity of the polygon 262 is confirmed by previous figure 35(a) and 35(b) obtained using the GCI and NDVI index. The red areas represent the most dense part of the sloping forest captured, with a very high value of stock volume. The polygon also has areas in which the density of trees is not very high, with few bare ground spots in the north-west part of the particle. This areas are correctly detected from both models, highlighting in blue color the parts with a low stock volume, with values tending towards zero. The difference in the results obtained through the models is minimum, since the stock volume macro patterns are recognized by both of them. From figure 35(b) is possible to notice that the model obtained through GNDVI index has a more narrow range of variability in the values but perhaps GCI model has a higher sensibility to low values, better described in figure 35(a). The application of the model derived from GNDVI could potentially lead to underestimation of biomass content.

To generalise the relationship between stock volume and spectral indices to a macro-area bigger than a particle, the mapping process is carried out considering the entire scene 15 as the framework. The following figure represents the spatial subset on which the volume is calculated, together with geographical references to the DTM of the area

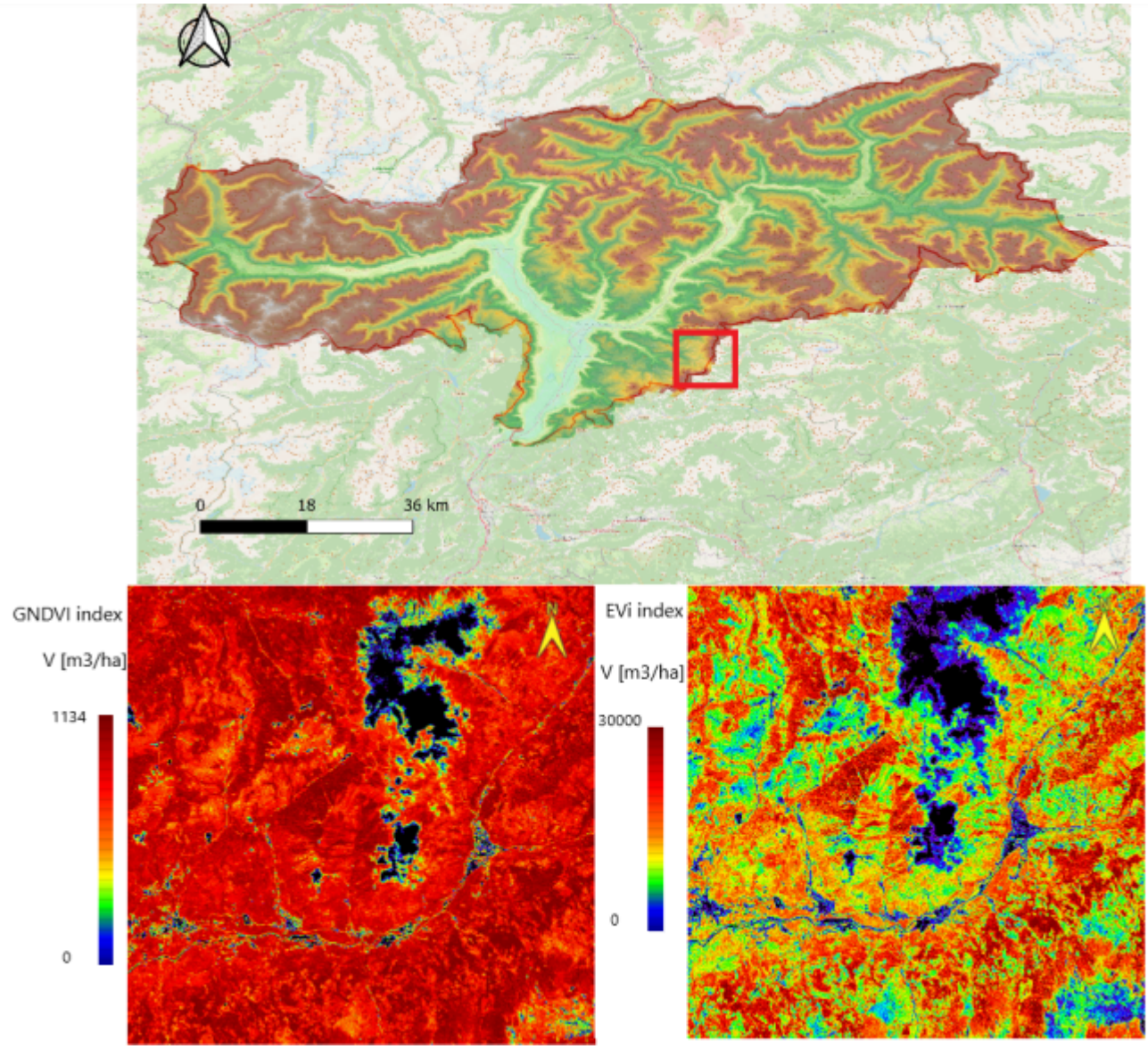


**Figure 36:** *Stock volume over the area of scene 15 using GCI and GNDVI index*

In the attempt to better highlight the areas with higher and lower volumes the results of the model's application is shown in the next figures supported by the linked real color image, for GCI model:

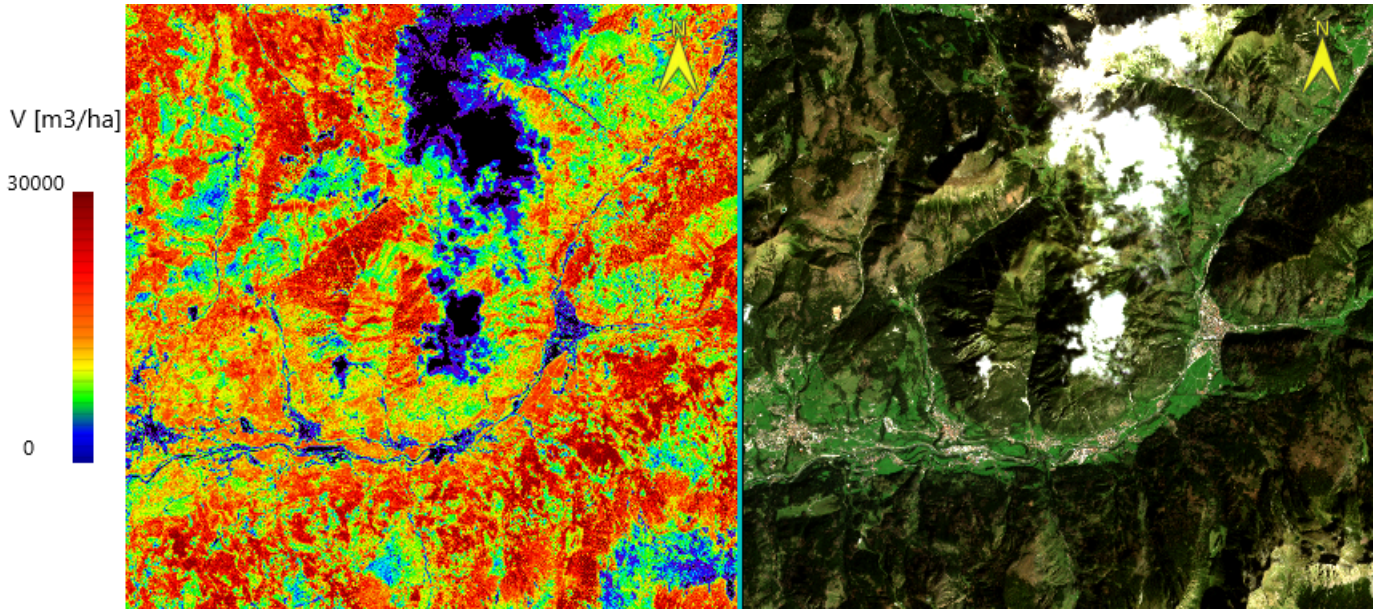


**Figure 37:** *Stock volume over the area of scene 15 using GCI index*

To compare the results with the real surfaces captured by the image, the link to the real-color image is represented on the right side of the image, showing the same spatial subset as the false color image. Also another image is displayed, estimating the stock volume with another index that shows strong correlation: GNDVI

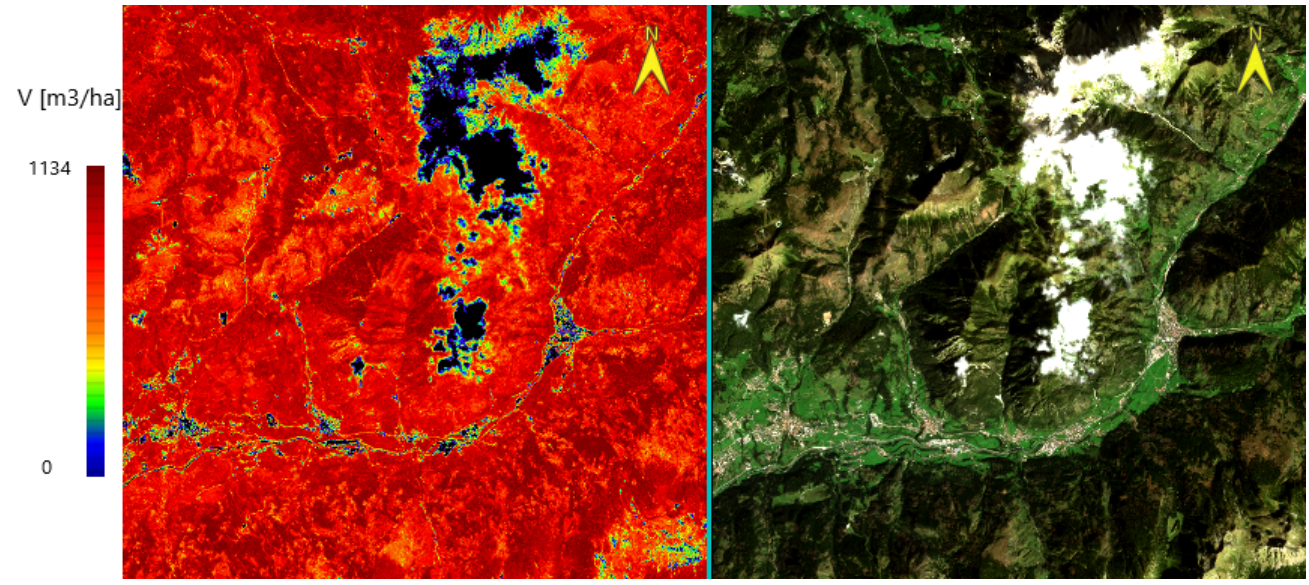


**Figure 38:** *Stock volume over the area of scene 15 using GNDVI index*

The volume's mapping obtained in figure 37 and figure 38 shows a good correlation with the actual presence of biomass observed. The area captured by scene 15 is characterized by vast grassland and forests with few villages and mountain crests, where the vegetation has very small density, these surfaces are correctly highlighted with the blue color, as in the valley part, where settlements and anthropic infrastructures are located. Analyzing figure 38, it appears grassland and bale grazing are considered areas with a high stock volume, values comparable to forests areas, which leads to the results that further

studies on the range of variation of biomass in both grassland and forest areas of Alto-Adige need to be assessed. Moreover, spots with very low reflectivity such as shady side of mountains, are associated with high stock volumes, which can not always be the case. Mountain crests and areas above the vegetation line, in the northern part of the image, are recognized successfully by both models as surfaces with very low stock volumes. As for the differences of the models obtained with GCI index and GNDVI index, figure 37 and 38 respectively, previous considerations apply, being GCI index model more sensitive to low values of volume.

Once the relationship between spectral indices and stock volume is obtained, the aim of the research is to elaborate a procedure that evaluates the biomass distribution over an alpine region, based on indices' values. Consequently the stock volume needs to be weighted considering each vegetation's specific value of WD and BEF(equation (6)). So in order to map these parameters values, a classification that considers the different species needs to be carried out. For collecting the images' samples that will be needed for the supervised classifications, the forestry field data are used once again, in particular the different abundance percentage are analyzed to select only the polygons that have a dominant vegetation type. Preliminary analysis show that collecting samples from each species is too specific thus very challenging because of the chaotic nature by which the different tree kinds distribute inside a forest, eventually the different types are unified into three groups out of which the regions of interest are acquired:

- Pine
- Spruce
- Other broadleved

The reflectivity statistics for each category are computed before different classification are applied:

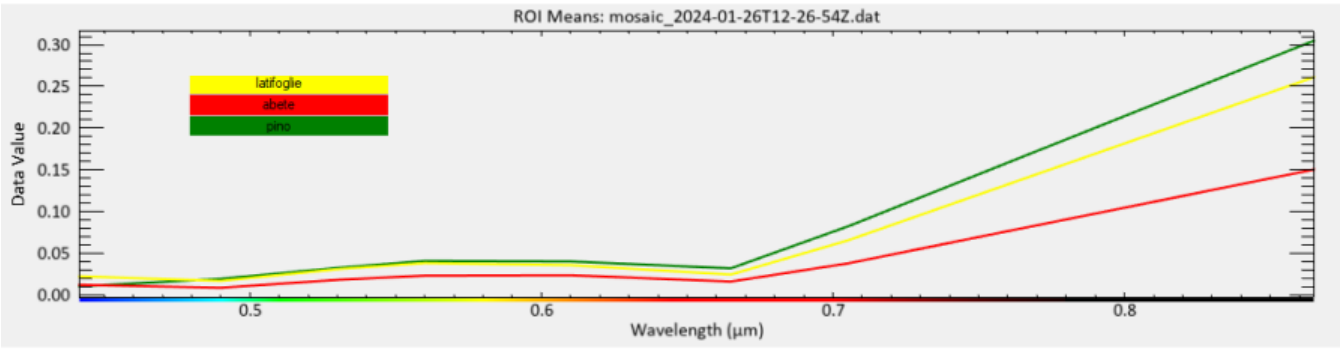


**Figure 39:** *Statistics of each vegetation class*

To better characterise each class, their footprint in the NIR band is represented:

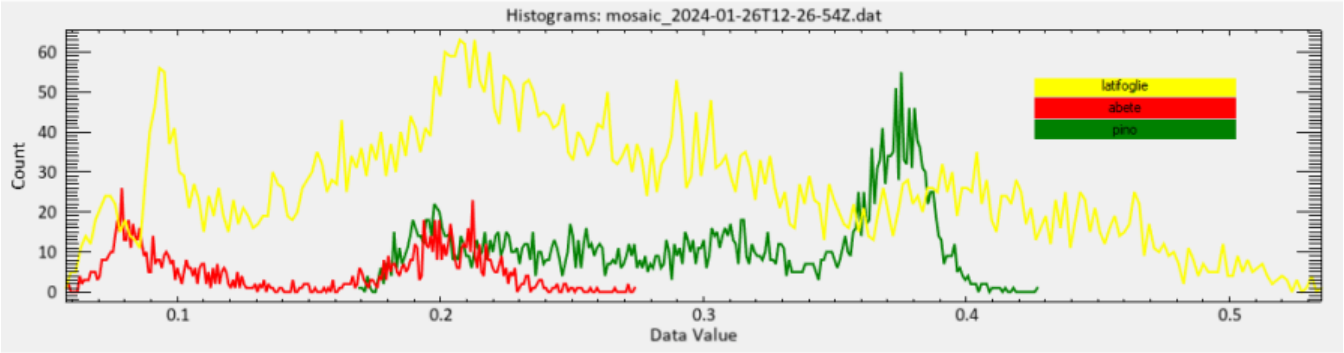


**Figure 40:** *Classes' footprint in NIR band*

Figure 40 shows the behavior of each vegetation type in the NIR band: pine's footprint ranges from 0.16 to 0.43 of reflectivity and has a pronounced spike around 0.37 values of NIR band; spruce's has two evident peaks around 0.04 and 0.2; broadleaved class has a wide range of variation but is characterized by high number of cells around reflectivity values of 0.1 and 0.2, the elevated noise by which broadleaved class is affected is caused by the high number of sample and of species that were incorporated in this class. The quality of the selected sample is assessed through ENVI's ROI Separability tool which computes the spectral separability between selected ROI pairs. Both the Jeffries-Matusita and Transformed Divergence separability measures are reported. These values range from 0 to 2.0 and indicate how well the selected ROI pairs are statistically separated.

```
Input File: mosaic_2024-01-26T12-26-54Z.dat
    ROI Name: (Jeffries-Matusita, Transformed Divergence)

latifoglie:
    abete: (1.92951099 1.99999984)
    pino: (1.99892163 2.00000000)

abete:
    latifoglie: (1.92951099 1.99999984)
    pino: (1.98156473 1.99752954)

pino:
    latifoglie: (1.99892163 2.00000000)
    abete: (1.98156473 1.99752954)

Pair Separation (least to most):

latifoglie and abete - 1.92951099
abete and pino - 1.98156473
latifoglie and pino - 1.99892163
```

**Figure 41:** *ROI separability*

Values greater than 1.9 indicate that the ROI pairs have good separability, in this case the pairs spruce-pine and broadleaved-pine has a very high value, greater than 1.98, instead for the broadleaved-spruce pair the separability is lower (1.93) but still considered acceptable.

## 4.3 Maximum likelihood classification

Maximum likelihood classification assumes that the statistics for each class in each band are normally distributed and calculates the probability that a given pixel belongs to a specific class. Each pixel is

assigned to the class that has the highest probability. Unless a probability threshold value is specified, all pixels are classified. If the highest probability is smaller than a threshold specified, the pixel remains unclassified, higher is the probability limit, and more pixel remain unclassified. For the purpose of the research, after few attempts, a threshold value of 0.6 is entered, the results of the classification follow:

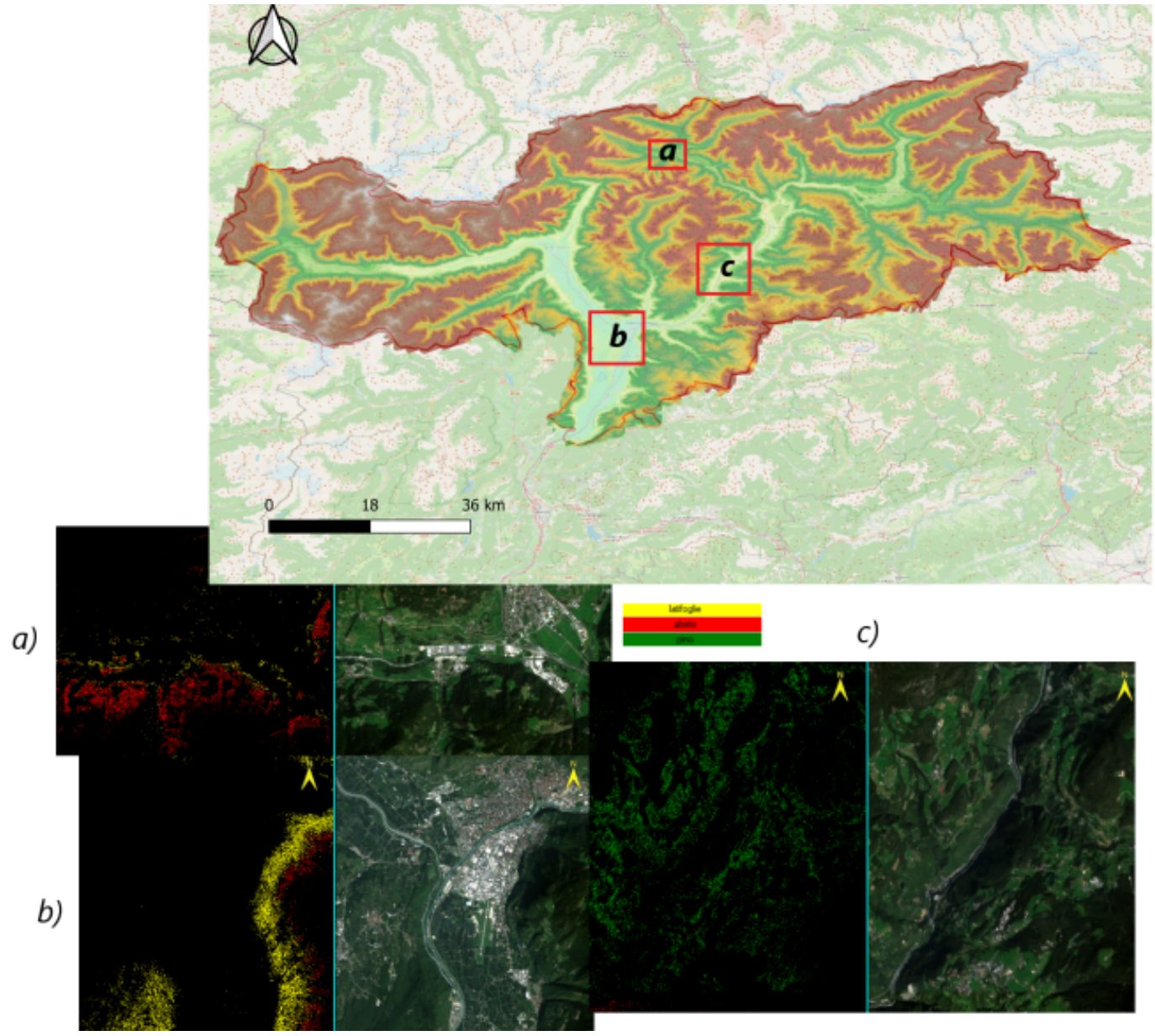


**Figure 42:** *Maximum likelihood classification*

From the results of the classification, can be noticed that the areas where each of the three vegetation types is dominant are recognized. The number of cells that remain unclassified is very high since 99.3% of all the pixels remain uncategorized, setting a lower threshold value would lead to a more inaccurate results, instead setting it to a higher value would bring into the results even more unclassified pixels. If globally the results could be considered of good quality, locally this classification would lead to an underestimation of the biomass available.

## 4.4 Minimum distance classification

The minimum distance technique uses the mean vectors of each class and calculates the Euclidean distance from each unknown pixel to the mean vector for each class. All pixels are classified to the nearest class unless a standard deviation or distance threshold is specified, in which case some pixels may be unclassified if they do not meet the selected criteria. The classification is performed selecting 4 as the standard deviation value, then this results are obtained:

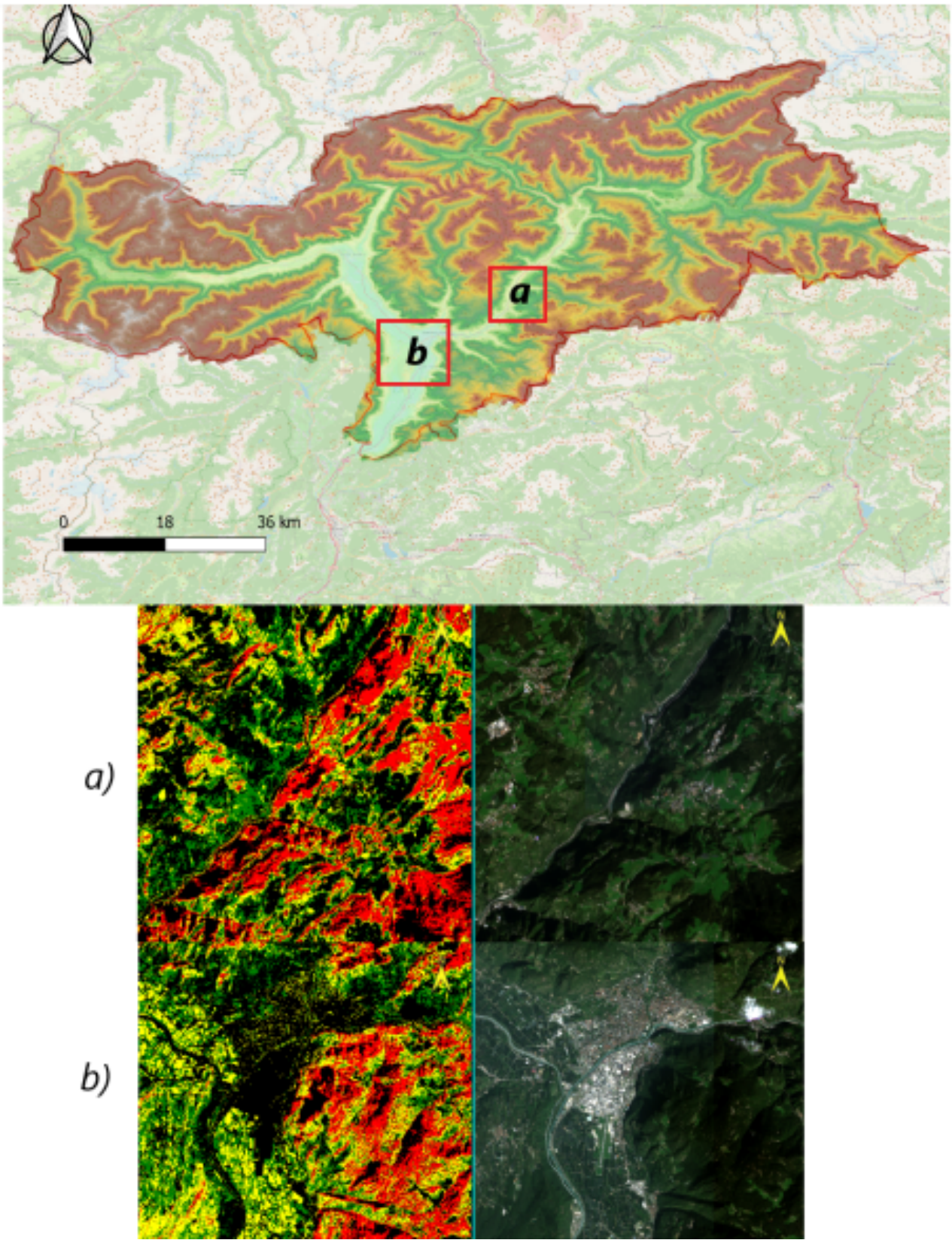


**Figure 43:** *Minimum distance classification*

From the results of the classification represented in figure 43(a) and 43(b) the area around the city of Bolzano and the Isarco valley are highlighted, together with their relative true color image. The results

show that this classification is able to assign pixels of the same area to different classes, leading to a more mixed output, respect to maximum likelihood classification. The number of unclassified cells is lowered to 84%, instead the most numerous class is considered the spruce class. It is interesting to notice that in figure 43(b), the shaded side of the valley is assigned mostly to the spruce class, which can reflect the natural behavior of this species into populating the more shaded and humid areas.

## 4.5 Spectral Angle Mapper classification

Spectral Angle Mapper (SAM) is a physically-based spectral classification that uses an n-D angle to match pixels to reference spectra. The algorithm determines the spectral similarity between two spectra by calculating the angle between the spectra and treating them as vectors in a space with dimensionality equal to the number of bands. This technique, when used on calibrated reflectance data, is relatively insensitive to illumination and albedo effects. Classes' spectra are directly extracted from the available scenes as region of interest (ROI) mean spectra. SAM compares the angle between the classes' spectrum vector and each pixel vector in 8 space. Smaller angles represent closer matches to the reference spectrum, for this reason the threshold angle set is equal to 0.1 rad. Pixels further away than the maximum angle threshold in radians are not classified.

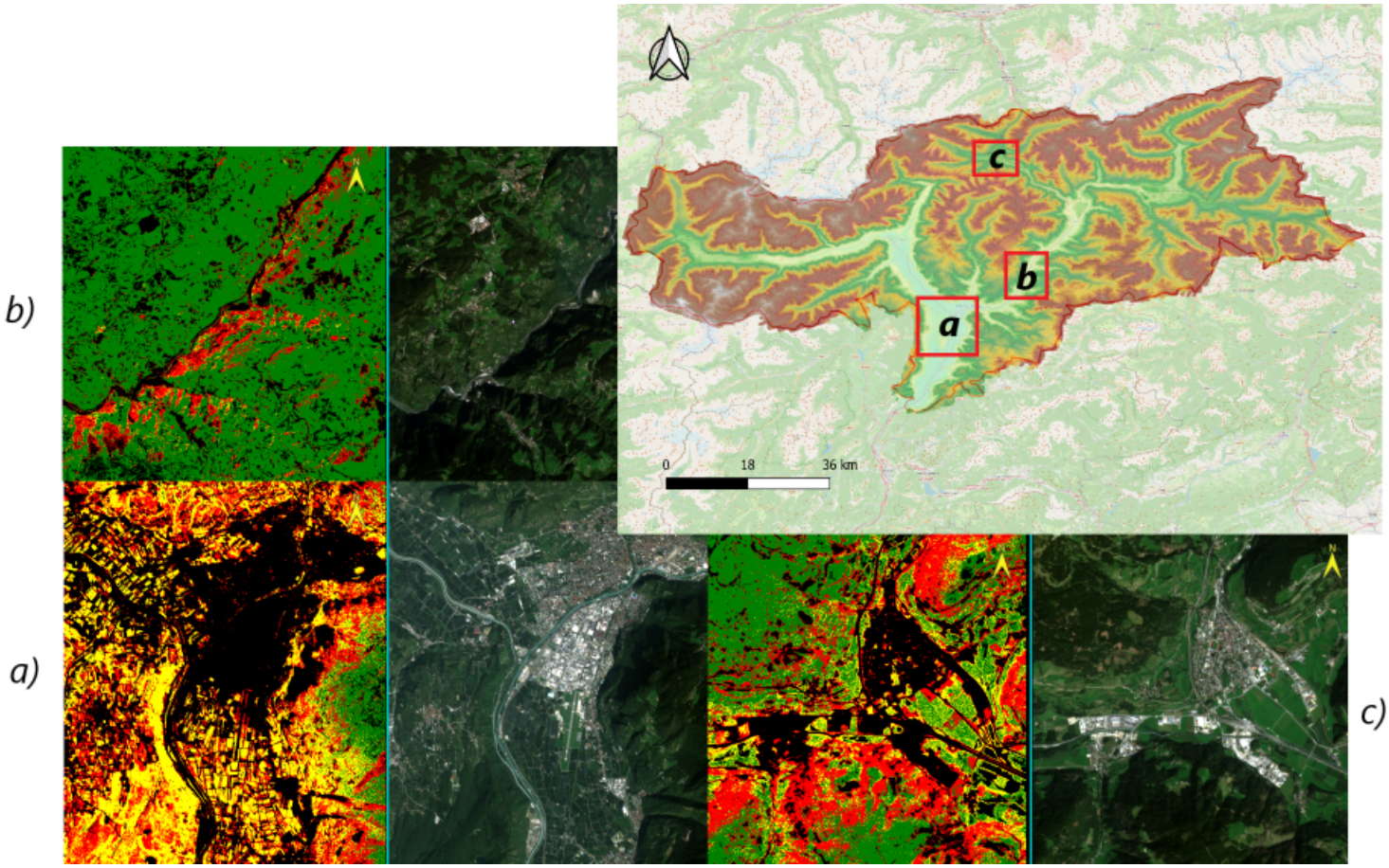


**Figure 44:** *SAM classification*

Comparing the outputs of SAM classification reported in figure 44(a), 44(b), 44(c) to the forest inventory data, a more detailed result is obtained respect to other classifications. The area around the city

of Bolzano is pictured in figure 44(a), the more abundant rainfall of this area offers a good environment for the presence of beech, which is dominant in this scene. At the low altitudes broadleaf forests popolate the mountains' slopes, among the most common species hophornbeam, temperate oak and locust are all grouped into the yellow class. In the Isarco valley 44(b), the majority of pixels are classified successfully, in fact a characteristic of the mesalpic district is the presence of Norway spruce, Scots pine and larch forest in the areas where beech trees are absent, also the high number of categorized pixel reflects the vegetation density o this area. Figure 44(c) shows the municipality of Bressanone, inside the transition endalpic area, Norway spruce is located mostly on the shady mountain's side. This species is common on the steep and shaded slopes and in the narrow valleys, is almost missing on the sunny slopes, with a prevalence of pixel assigned to the pine class on this surfaces. Locally it is very frequent to find broadleaved trees, especially in the low altitudes of the valleys around the main Alpine range, such as the municipality of Vipiteno captured in figure 44(c). The overall number of categorized pixel is acceptable, with the majority of them (86%) falling in class pine, represented in green in the false color images.

## 4.6 Biomass estimation

The results of the estimation of biomass over the study areas will be presented in this section. Considering the previous examinations, SAM algorithm results in the most precise categorization of the pixels. The classification was carried out over the whole scene and in detail for the example particle n°262 the following result is obtained:

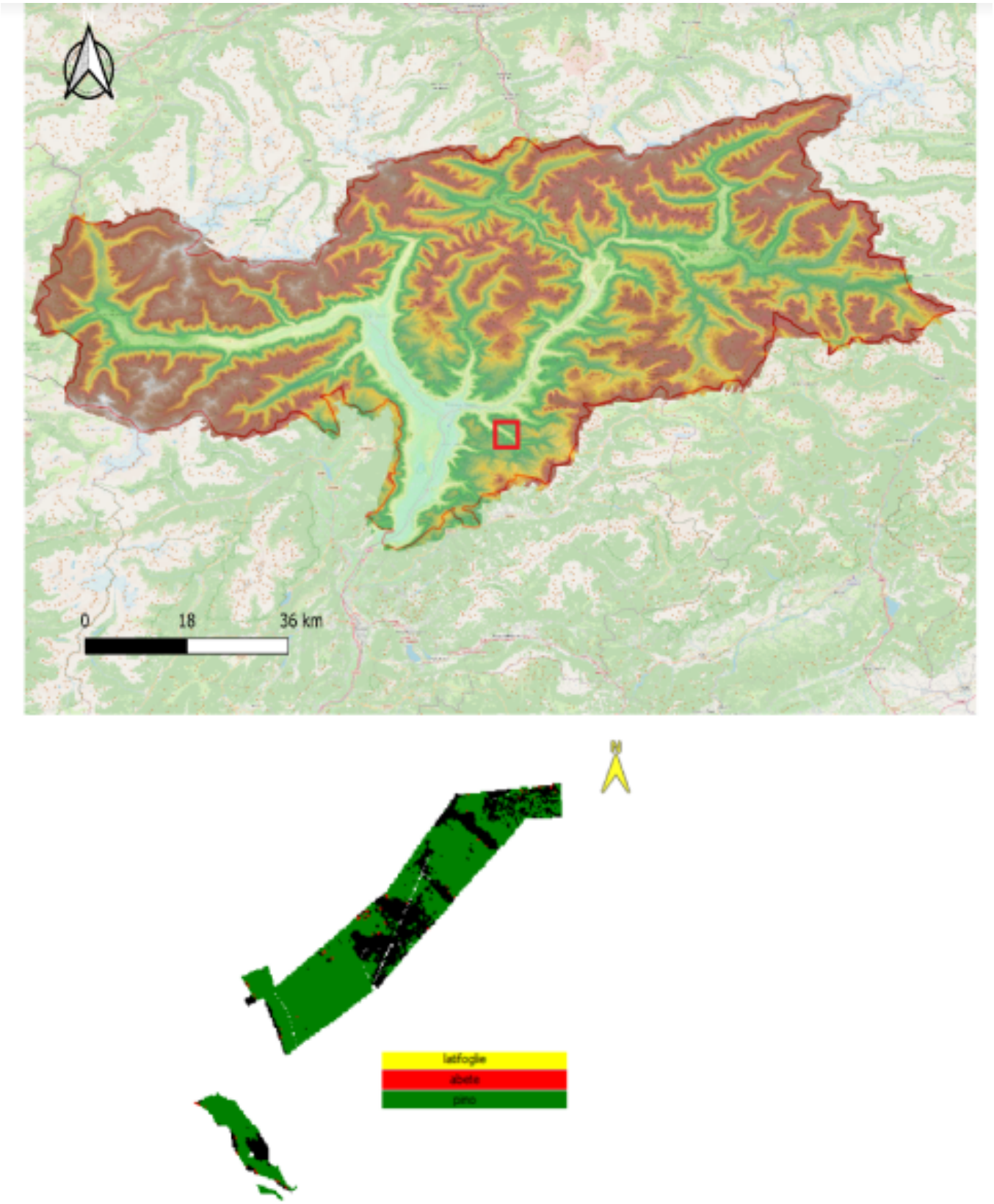


**Figure 45:** *SAM classification for particle 262*

Consulting the forest inventory data, the particle 262 is composed by:

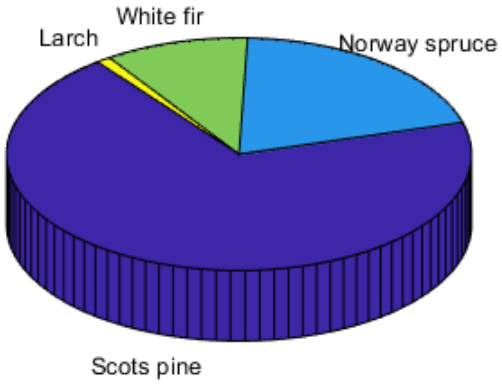


**Figure 46:** *Vegetation species on the area*

- 69%: Scots pine
- 20%: Norway spruce
- 10%: white fir
- 1%: larch

The classification's results reported in previous figure reflect the ground reality pictured in figure 33, dense pine vegetation ranges from the lower to the upper part of the slope, representing the majority of the tree species. In the central and upper part of the polygon few bare ground spots are present, being correctly assigned to the *unclassified* class. Few points falling in the *spruce* class populate the particle as the second most diffused type. Each class of the categorized image is assigned to the relative values of BEF and WD factors, as specified in table 3, then through ENVI's *band math operation* equation (6) is applied to the whole scene in order to obtain the mapping of AGB values. Two different results are obtained, the first evaluation (a) took into account the stock volume obtained through GCI index model in figure 35(a), the second (b) considered the stock volume obtained through GNDVI index model in figure 35(b):

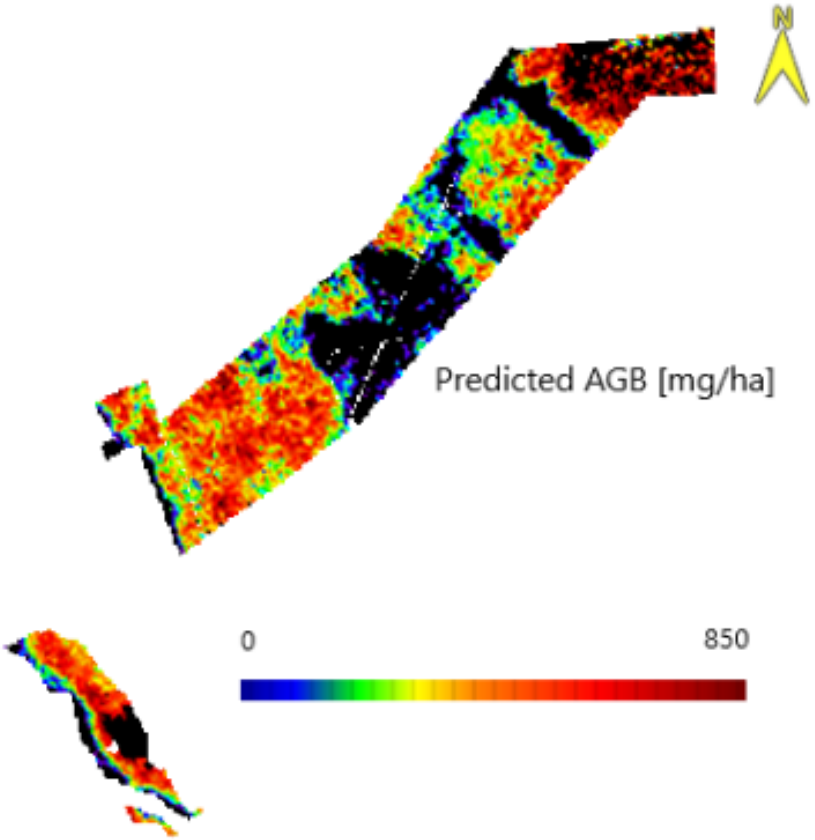


**(a)** *Spatial distribution of AGB for particle 262 through GCI index*

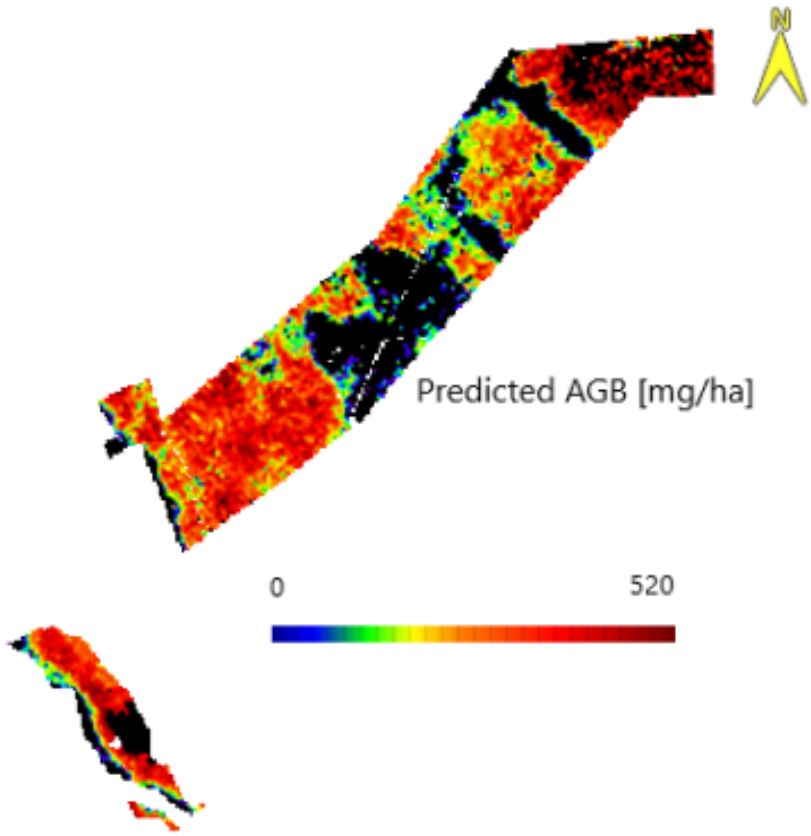


**(b)** *Spatial distribution of AGB for particle 262 through GNDVI index*

**Figure 47:** *Biomass distribution over particle 262*

The results obtained for particle 262 displayed in previous figures are considered realistic, highlighting the parts characterised by the highest AGB values as the areas with dense Scots pine forests and recognized with very low AGB values the areas with bare ground. Small discrepancy between the two models are visible, as the GNDVI index model results in a lower overall estimation of biomass, leading possibly to an underestimation over the particle. Expanding the results over the whole PlanetScope data set, AGB is obtained for all the scenes, the following representations are achieved for scene 15:

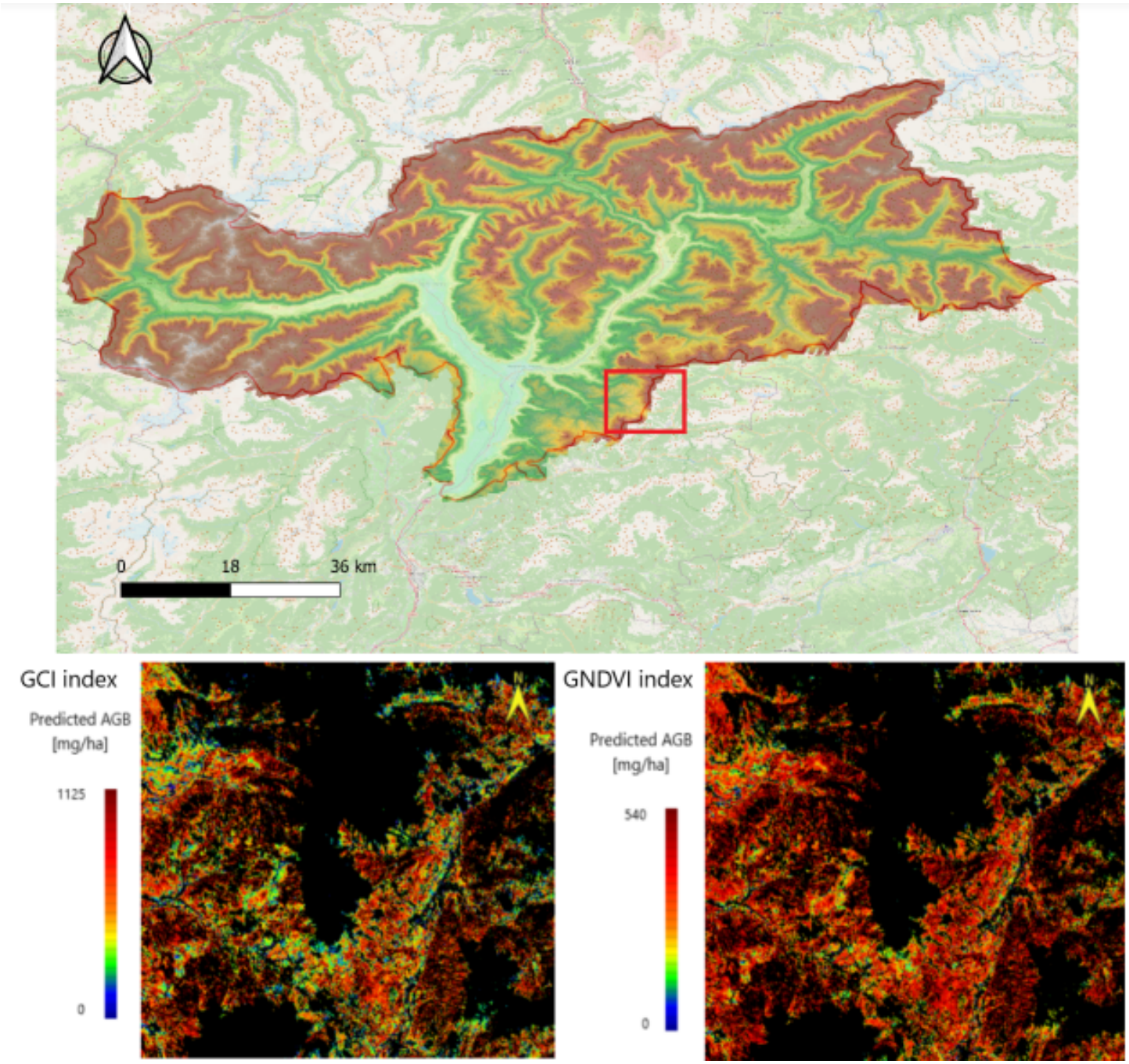


**Figure 48:** *Spatial distribution of AGB for scene 15 using GCI and GNDVI index model*

Along with a more detailed view, sided by the real color image of the area represented:

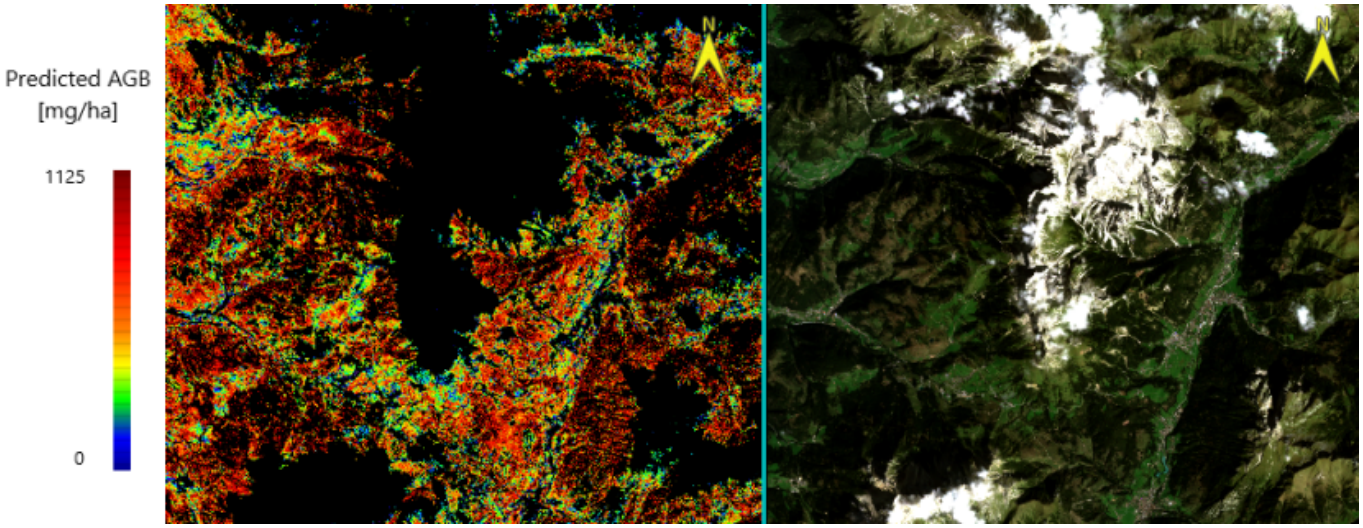


**Figure 49:** *Spatial distribution of AGB for scene 15 using GCI index model*

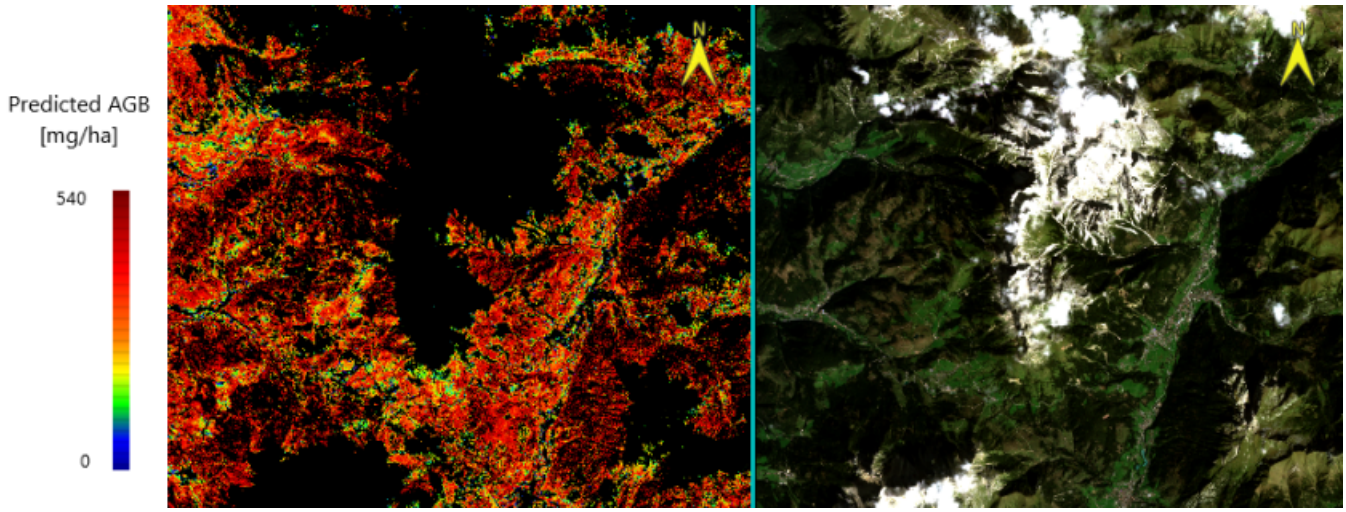


**Figure 50:** *Spatial distribution of AGB for scene 15 using GNDVI index model*

The application of the models over a vast area gives satisfying results as in can be seen in figure 49 and 50 for scene 15. Glaciers and mountain crests as anthropic construction and villages are correctly identified as surfaces with very low to null biomass presence. Dense Norway spruce and Scots pine are labelled with high values of AGB just as it was expected. It is interesting to notice in figure 49 the accurateness by which sub-mountain bale grazing and grassland areas are assigned to intermediate values of AGB by the application of GCI index model, being more sensitive to low stock volumes as commented in previous section.

# 5 Discussion

The aim of the study is to elaborate a model that is able to estimate the carbon stocks of an alpine area, through the AGB quantification, being biomass a key quantity when estimating terrestrial stock amount. The increasing demand for methodologies able to make such estimation is driven by the interest

of many companies in the stock market investments. The acquisition of stocks would allow businesses to compensate their emission total, funding reforestation and other environmental projects. The key point in the market development is the possibility to assign a realistic value to the single stocks, through quantitative environmental related variable such as the above ground biomass and stock volume a correct correspondence could be obtained, assuring the investors of the effective value of their purchase.

Remote sensing techniques allow to obtain an effective dataset for biomass estimation, their application offers important advantages in this field, as the possibility to acquire off grid data with high resolution and with low time consumption, at a relatively low cost, respect to field surveys. In the same alpine area of Trentino Alto-Adige, other studies tried to estimate biomass content through SAR and LiDAR data [11], assessing the challenges of each methods. No previous studies analysed the possibility to use high resolution optical data for this purpose. The available optical dataset obtained through PlanetScope missions allows to have a high geometrical resolution (3 m) of the 8 bands acquisitions, which allows a detailed analysis at the regional scale, considering municipal particles as the fundamental units. The optical data is compared to the accessible forest inventory data, collected on the field by the local authorities. Forestry inventory data needed to be analyzed and selected, as missing information or imprecise data were common over the polygons. Eventually allometric relationships, whose consider species related characteristics, were used to transit from stock volume to AGB value, the research focused then on the stock volume mapping, since it was found to be the main parameter on which biomass depends on. Volume data coupled with the mean spectral indices value for each unit are used for the models' calibration.

Among the spectral indices utilised, GCI index and GNDVI index show the highest correlation with particles' biomass content. The prediction phase, in which the models' output are compared to the field data, allows to assess the quality of the models and confirms that indices such as LAI and NDVI leads to very inexact results. More specific indices such as GCI, GNDVI or EVI ended up to be more suitable for this application in the alpine and mountainous environment. From the stock volume maps obtained in figure 37 and 38, the research tried to obtain the biomass distribution over the whole area. Different supervised classification algorithms are used to categorize each pixel of the image, in order to associate the stock volume data with species related parameters. The selected regions of interest relate to the dominant vegetation types in the region: pine, spruce and all the other types grouped in the broadleaved class. Spectral angle mapper (SAM) classification returns the most accurate subdivision, which can be considered reliable at regional scale but less accurate at particle scale. Being the ROIs separability index very high, perhaps the imprecision source could be attributed to the evaluation of the species found inside a polygon.

## 5.1 Limitations

The application of the models over the region recognized correctly where most of the biomass presence in concentrated, at local scale though the quality of the AGB estimation returns values that could be certainly improved by a better understanding of site's ecosystem and local characteristics. The main limitation of the study is the low accuracy by which classification algorithms assign each pixel to their correct tree category, especially at a high level of detail commonly required to characterise municipal scale studies. The ROIs separability index demonstrated that the samples were very distinguishable so the inaccurateness could be linked to the low reliability of the forestry inventory data, more dense and precise field data could also improve the calibration process. The most important source of such additional uncertainty is that forest inventory evaluation typically focus only on commercially important stem volume and rarely include quantitative estimates of other important biomass components, making it necessary to estimate these elements of total biomass using conversion and expansion factors. The Intergovernmental Panel on Climate Change (IPCC) developed different reports on good practice guidance for land use, land-use change and forestry (LULUCF), in which the evaluation of these factors are given for various conditions and environments, providing supplementary methods and good practice guidance for estimating, measuring, monitoring and reporting on carbon stock changes and greenhouse gas emissions. However, country specific factors are often lacking sometimes even at national levels, but more often at regional levels. For a precise biomass estimation forestry inventory campaigns not only need to be carried out at regional scale but they also need to be updated frequently: even if the forest biomass increment is slow in time, timber management activities can alter the forest volume and cause errors if old biomass or volume data are used; consequently, using updated data is critical.

Another uncertainty source is that the factors to be used are usually species specific [24], however they may also depend on site [25], forest history and tree size or age [27], because these all affect the biomass allocation strategies of the trees [24]. The average values reported by the literature [27, 28] are available only for the main species or species groups. In addition to the fact that specific data are lacking for many species, the application of these parameters include also uncertainties due to missing information concerning stand structure, age and compartments included in the values.

The application of these models needs to considered that the results obtained, along with indices interpretation, utilised very specific species and site factors that allow to consider the validity of the research limited to the alpine and sub-alpine environment in which the study was carried out. For a more general application, index-based models need to be properly calibrated, for the different biomass content of the image, for instance a certain EVI index value can be considered low for forest areas but extremely high for grassland surfaces.

An important challenge in the biomass evaluation of the alpine area is the asperity of the territory that alternates between very steep slopes, in which distortion effects may be introduced in the acquisitions, and narrow valley, where sun exposure is very limited. In particular the maps obtained in figure 49 and

50, show a possible overestimation of biomass content on the shaded slopes, further studies need to be carried out for assessing biomass content difference between sunny and shady side of the mountains.

# 6 Conclusion

Figure 49 and 50 represent the AGB distribution obtained over scene 15, the GCI and GNDVI index models produce similar results, being able to recognize the main patterns in the biomass variation. GCI index model was found to be able to better distinguish between areas with higher biomass content, such as pine and spruce forests, and surfaces with a low to moderate level of AGB, respect to GNDVI index model, and may be due to the model's inability to represent the differentiation in forest structure that occurs within the forest. Figure 38 shows the stock volume estimation over scene 15 through GNDVI index model, the displayed results suggest that AGB calculation could be affected by saturation problems at high values of stock volume. The application of GNDVI index model leads though, to AGB values closer to those obtained through forest inventory data.

To achieve better biomass estimation Lidar data could be a valuable source, in fact Trentino Alto-Adige region is among the regions with the highest Lidar coverage. The availability of a well managed and updated Lidar dataset, together with proper ground data to calibrate the Lidar-based model, could solve most limitations. Furthermore, a Lidar dataset would be beneficial for many other applications, including hydrogeological and risk assessment models, or biodiversity assessments. PlanetScope dataset offered a higher spatial resolution, compared to Sentinel-2 and Landsat 8 OLI, which allowed to improve the accuracy of AGB estimates [16], and may have enabled a better separation of tree species with varying canopy greenness, which led to the greater model precision achieved.

Continuous monitoring is required to determine the role of alpine forests in the global carbon cycle, having Alto-Adige region one of the richest biomass presence on the italian territory. The accuracy of estimates was increased by using remote sensing data for AGB estimation. Therefore, by increasing precision, the remote sensing-based methodologies used in this study will complement the field-based estimates of AGB. Suggesting the most effective way for making accurate evaluations is to use various sources of data. The study eventually aims to give an insight into methods for a correct carbon stock assessment, leading to the implementation of remote sensing technologies into the stock market field. Future research should therefore concentrate on improving these restrictions by employing the synergy of various data sources to increase the estimation efficiency of AGB models beyond what was achieved in the current work.

# 7 Bibliography

[1] Liao, Y.; Zhang, J.; Bao, R.; Xu, D.; Han, D. Modelling the Dynamics of Carbon Storages for Pinus densata Using Landsat Images in Shangri-La Considering Topographic Factors. Remote Sens. 2022, 14, 6244.

[2] Zhang, B.; Li, X.; Du, H.; Zhou, G.; Mao, F.; Huang, Z.; Zhou, L.; Xuan, J.; Gong, Y.; Chen, C. Estimation of Urban Forest Characteristic Parameters Using UAV-Lidar Coupled with Canopy Volume. Remote Sens. 2022, 14, 6375.

[3] Li, L.; Zhou, B.; Liu, Y.; Wu, Y.; Tang, J.; Xu, W.; Wang, L.; Ou, G. Reduction in Uncertainty in Forest Aboveground Biomass Estimation Using Sentinel-2 Images: A Case Study of Pinus densata Forests in Shangri-La City, China. Remote Sens. 2023, 15, 559.

[4] Vahidi, M.; Shafian, S.; Thomas, S.; Maguire, R. Estimation of Bale Grazing and Sacrificed Pasture Biomass through the Integration of Sentinel Satellite Images and Machine Learning Techniques. Remote Sens. 2023, 15, 5014.

[5] Huang, Q.; Lu, X.; Chen, F.; Zhang, Q.; Zhang, H. High-Resolution Remote Sensing Images Can Better Estimate Changes in Carbon Assimilation of an Urban Forest. Remote Sens. 2023, 15, 71.

[6] Chinembiri, T.S.; Mutanga, O.; Dube, T. Landsat-8 and Sentinel-2 Based Prediction of Forest Plantation C Stock Using Spatially Varying Coefficient Bayesian Hierarchical Models. Remote Sens. 2022, 14, 5676.

[7] Zhou, L.; Li, X.; Zhang, B.; Xuan, J.; Gong, Y.; Tan, C.; Huang, H.; Du, H. Estimating 3D Green Volume and Aboveground Biomass of Urban Forest Trees by UAV-Lidar. Remote Sens. 2022, 14, 5211.

[8] Gao, L.; Chai, G.; Zhang, X. Above-Ground Biomass Estimation of Plantation with Different Tree Species Using Airborne LiDAR and Hyperspectral Data. Remote Sens. 2022, 14, 2568.

[9] Liu, Z.; Michel, O.O.; Wu, G.; Mao, Y.; Hu, Y.; Fan, W. The Potential of Fully Polarized ALOS-2 Data for Estimating Forest Above-Ground Biomass. Remote Sens. 2022, 14, 669.

[10] Schino, G., Borfecchia, F., De Cecco, L. et al. Satellite estimate of grass biomass in a mountainous range in central Italy. Agroforestry Systems 59, 157–162 (2003).

[11] Vaglio Laurin, G.; Puletti, N.; Tattoni, C.; Ferrara, C.; Pirotti, F. Estimated Biomass Loss Caused by the Vaia Windthrow in Northern Italy: Evaluation of Active and Passive Remote Sensing Options. Remote Sens. 2021, 13, 4924.

[12] Kumar, L.; Mutanga, O. Remote Sensing of Above-Ground Biomass. Remote Sens. 2017, 9, 935.

[13] Li, Y., Li, M., Li, C. et al. Forest aboveground biomass estimation using Landsat 8 and Sentinel-1A data with machine learning algorithms. Sci Rep 10, 9952 (2020).

[14] Tian, L.; Wu, X.; Tao, Y.; Li, M.; Qian, C.; Liao, L.; Fu, W. Review of Remote Sensing-Based Methods for Forest Aboveground Biomass Estimation: Progress, Challenges, and Prospects. Forests 2023, 14, 1086.

[15] Csillik, O.; Kumar, P.; Asner, G.P. Challenges in Estimating Tropical Forest Canopy Height from Planet Dove Imagery. Remote Sens. 2020, 12, 1160.

[16] Sami D. Madundo, Ernest W. Mauya, Charles J. Kilawe, Comparison of multi-source remote sensing data for estimating and mapping above-ground biomass in the West Usambara tropical montane forests, Scientific African, Volume 21, 2023.

[17] Brown, S.; Lugo, A.E. Aboveground biomass estimates for tropical moist forests of the Brazilian Amazon. Interciencia Caracas 1992, 17, 8–18.

[18] Della Valle, E. Valutazione dello Stock di Carbonio e delle Capacità Fissative delle Foreste Assestate e dei Boschi di Neoformazione nella Regione Veneto. Ph.D. Thesis, University of Padova, Padova, Italy, 2008.

[19] Teobaldelli, M.; Somogyi, Z.; Migliavacca, M.; Usolt-sev, V.A. Generalized functions of biomass expansion factors for conifers and broadleaved by stand age, growing stock and site index. For. Ecol. Manag. 2009, 257, 1004–1013.

[20] Huang, X.; Xiao, J.; Wang, X.; Ma, M. Improving the global MODIS GPP model by optimizing parameters with FLUXNET data. Agric. For. Meteorol. 2021, 300, 108314.

[21] George E. Meyer, João Camargo Neto, Verification of color vegetation indices for automated crop imaging applications, Computers and Electronics in Agriculture, Volume 63, Issue 2, 2008.

[22] Khodakarami, L., Pourmanafi, S., Soffianian, A. R., & Lotfi, A. (2022). Modeling spatial distribution of carbon sequestration, CO2 absorption, and O2 production in an urban area: Integrating ground-based data, remote sensing technique, and GWR model. Earth and Space Science, 9, e2022EA002261

[23] Wang, J.; Xiao, X.; Bajgain, R.; Starks, P.; Steiner, J.; Doughty, R.B.; Chang, Q. Estimating leaf area index and aboveground biomass of grazing pastures using Sentinel-1, Sentinel-2 and Landsat images. ISPRS J. Photogramm. Remote Sens. 2019, 154, 189–201.

[24] Levy, Peter. (2004). Biomass expansion factors and root : shoot ratios for coniferous tree species in Great Britain. Forestry. 77. 421-430. 10.1093/forestry/77.5.421.

[25] Wirth C, Schumacher J, Schulze ED. Generic biomass functions for Norway spruce in Central Europe–a meta-analysis approach toward prediction and uncertainty estimation. Tree Physiol. 2004

[26] Mutanga, O., & Skidmore, A. K. (2004). Hyperspectral band depth analysis for a better estimation of grass biomass, Cenchrus ciliaris, measured under controlled laboratory conditions. International Journal of Applied Earth Observation and Geoinformation (JAG), 5(2), 87-96.

[27] IPCC, 2003, Good Practice Guidance For Land Use, Land-Use Change and Forestry.

[28] IPCC, 2006, IPCC Guidelines for National Greenhouse Gas.

[29] Provincia autonoma di Bolzano <https://www.provincia.bz.it/agricoltura-foreste/bosco-legno-malghe>

[30] Planet. Developers portal <https://developers.planet.com>